Revision 2

Analysis of hydrogen and fluorine in pyroxenes: Part I. Orthopyroxene

JED L. MOSENFELDER* and GEORGE R. ROSSMAN

[1]Division of Geological and Planetary Sciences, California Institute of Technology, M/C 170-25, Pasadena, California 91125-2500, U.S.A.

*E-mail: jed@gps.caltech.edu

ABSTRACT

We measured trace concentrations of hydrogen (~40-400 ppm H_2O) and fluorine (<1 to 17 ppm) in a suite of nine orthopyroxenes from varying geological environments, using secondary ion mass spectrometry (SIMS). The SIMS data for H (measured as $^{16}O^{1}H$, referenced to ^{30}Si and ^{18}O) are cross calibrated against Fourier transform infrared (FTIR) spectra, in turn calibrated against either manometry (Bell et al. 1995) or the frequency dependent molar absorption coefficient derived by Libowitzky and Rossman (1997). Despite the fact that our samples exhibit a wide range of IR band structures, with varying percentages of absorbance split among low (2600-3350 cm^{-1}) and high (3350-3700 cm^{-1}) wavenumber bands, our SIMS data are fit with the same precision and virtually the same regression slope regardless of which IR calibration is used. We also confirm previous suggestions that the matrix effect for SIMS analyses between orthopyroxene and olivine is small (≤20%). Anomalously high yields of $^{16}O^{1}H$ in some analyses can be attributed to the presence of amphibole lamellae, and these analyses must be filtered out with different criteria than for olivine due to differences in the geometrical relationship of host to inclusion. For F, our derived values are highly dependent on analytical uncertainties related to the use of silicate glasses as standards. Regardless of the accuracy of our calibration, we see systematic differences in F concentrations in orthopyroxenes and olivines depending on their geological context. Samples derived from crustal environments and from Colorado Plateau minette diatremes have very low F (≤3 ppm), while higher contents can be found in megacrysts from South African kimberlites (up to 17 ppm in orthopyroxene and 47 ppm in olivine) and in xenocrysts from the Rio Grande Rift (Kilbourne Hole, 7-9 ppm in orthopyroxene).

Keywords: FTIR, SIMS, mantle, calibration, nominally anhydrous minerals

INTRODUCTION

It is now firmly established that the major rock-forming minerals of the Earth's upper mantle – olivine, orthopyroxene, clinopyroxene, and garnet – have the capacity to incorporate hydrogen into their structures in the form of structurally bound hydroxide groups, at levels ranging from trace amounts (Bell and Rossman 1992) up to thousands of ppm H_2O (Kohlstedt et al. 1996; Mosenfelder et al. 2006a; Smyth et al. 2006; Mierdel et al. 2007; Withers and Hirschmann 2008; Withers et al. 2011). Accurate modeling of processes influenced by H in these nominally anhydrous minerals (NAMs) – such as deformation and melting – relies on accurate measurement of H in both natural and experimentally produced samples. Some recent studies of natural samples have focused on pyroxenes, which typically have more H than coexisting olivine – sometimes to a degree unexpected from experimental partitioning data (Peslier and Luhr 2006). This implies that pyroxenes better retain H during decompression and cooling compared to olivine. Based on this inference, they are thus a better choice for estimating the water content of the magma from which they crystallized or of the solid source from which they were extracted (Peslier et al. 2002; Wade et al. 2008; Gose et al. 2009; Warren and Hauri 2010; Nazzareni et al. 2011; Sundvall and Stalder 2011). On the experimental side, considerable progress has been made towards determining storage capacities, incorporation mechanisms, and diffusion rates for H in clinopyroxene and orthopyroxene, particularly in the latter (Rauch and Keppler 2002; Stalder 2004; Stalder and Skogby 2002, 2003; Stalder et al. 2005, 2007; Mierdel and Keppler 2004; Mierdel et al. 2007).

In addition to H, recent studies have shown that pyroxenes can contain – apparently as structurally bound entities, not just in inclusions – significant amounts of

boron, fluorine, and chlorine (Hervig and Bell 2005; Hauri et al. 2006a; Hålenius et al. 2010; O'Leary et al. 2010; Bernini et al. 2012; Beyer et al. 2012; Dalou et al. 2012). Due to their high solubility in aqueous fluid and/or silicate melts, these light elements are also of interest to geochemists for understanding chemical recycling and melting processes in the Earth and other planetary bodies. Recently reported concentrations in synthetic pyroxenes range up to 2000 ppm B (Hålenius et al. 2010), 600 ppm F (Dalou et al. 2012), and 80 ppm Cl (Dalou et al. 2012). Moderate amounts of F have also been identified in pyroxene (and olivine) megacrysts from kimberlites (Hervig and Bell 2005; Guggino et al. 2007; Mosenfelder et al. 2011; Beyer et al. 2012). These studies used low-blank methods with high sensitivity and the capability to discriminate surface contamination: B was measured by nuclear reaction analysis (NRA), and F and Cl were measured with secondary ion mass spectrometry (SIMS).

In this study, we focus on quantification of H and F in pyroxenes using two techniques, Fourier transform infrared (FTIR) spectroscopy and SIMS. Our results on orthopyroxene and clinopyroxene are presented in parts I and II, respectively. FTIR is a well-established technique used routinely for measuring H (but not commonly used for F). However, significant problems remain with accurate quantification using this method. The utility of SIMS for measuring H and F in minerals has been long recognized (Hinthorne and Andersen 1975). However, measurement of low H concentrations, such as in many natural NAMs, has only recently become tractable as a result of advances in instrumentation, analytical protocols, and sample preparation techniques (Kurosawa et al. 1997; Hauri et al. 2002; Koga et al. 2003; Aubaud et al. 2007). Here we present SIMS data on simultaneously measured H and F in nine different orthopyroxenes, acquired

using the methods outlined in Mosenfelder et al. (2011). We also compare these data to measurements taken on olivine during the same session, as well as calibrations presented by other laboratories. We assess possible sources of analytical uncertainties for both SIMS and FTIR, examine the possibility that the IR absorption coefficient for O-H bonds is frequency dependent, and finally discuss implications of our work for F distribution in the Earth's mantle and crust.

ANALYTICAL METHODS

Sample preparation, electron probe microanalysis (EPMA), and FTIR

The orthopyroxenes and glasses we analyzed are listed in Tables 1 and 2, respectively; details on the olivine samples are in Mosenfelder et al. (2011). Sample preparation and cleaning protocols followed the methods in Mosenfelder et al. (2011). Minerals were oriented for polarized FTIR measurements using optical methods (examination of cleavage, morphology, pleochroism, and extinction/interference figures under cross polarized light). Spindle stage methods, used for orienting clinopyroxene in part II of the study, were not necessary for the orthopyroxenes used here, many of which were large gem-quality crystals. A single exception is sample KBH-1, oriented by Bell et al. (1995). We estimate the accuracy of orientations to be ±2°, with the major source of uncertainty coming from cutting and polishing. Orientations were also confirmed using silicate overtone spectra, examples of which are shown in the appendix. We follow the conventions $\alpha = n_\alpha = X \parallel [010] \sim 9$ Å, $\beta = n_\beta = Y \parallel [100] \sim 18.3$ Å, and $\gamma = n_\gamma = Z \parallel [001] \sim 5.2$ Å, and use the Greek letters to designate polarized spectra with the **E** vector parallel to the given optic/crystallographic direction.

Our procedures for EPMA and FTIR spectroscopy have been described previously (Mosenfelder et al., 2006a; 2006b; 2011). EPMA data are presented in Table 3 and FTIR data are included in Table 1. Most FTIR spectra were acquired in the main compartment of the spectrometer with light polarized by a $LiIO_3$ Glan-Foucault prism; some spectra were taken in the microscope. Furthermore, a CaF_2 wire-grid polarizer was used in some cases, which allowed us to measure absorbance in both the silicate overtone and OH-vibrational regions (see appendix). Spectra taken with these different experimental setups were consistent where comparisons were made. Details of our baseline correction methods are discussed in the appendix and the baselines (and corrected spectra) are provided in the supplementary material.

Hydrogen concentrations (given as ppmw H_2O) were determined from FTIR data using the Beer-Lambert law and two different calibrations for the integrated molar absorption coefficient (ε_i): the manometry based calibration of Bell et al. (1995) and the generic, wavenumber dependent calibration of Libowitzky and Rossman (1997). The value for ε_i is 80,600±3200 (1σ) l mol^{-1}_{H2O} cm^{-2} in the former case, while in the latter ε_i (in l mol^{-1}_{H2O} cm^{-2}) = 246.6(3753-ν), where ν is wavenumber in cm^{-1}.

Sample densities were measured for most samples via Archimedes' method using immersion in toluene, and these values were used in the estimation of H concentrations. For some samples that were too small and/or fractured to measure accurately this way, we assumed the same density as measured by Bell et al. (1995) for KBH-1 (3.318 Mg/m^3). The measured differences in density between our samples (Table 1) result in very little change in the final estimated H concentrations, on the order of 1-2 ppm H_2O compared to assuming the same calibration factor derived for KBH-1.

Final uncertainties in H concentrations calculated using the Bell et al. (1995) calibration were estimated by propagating the 2σ uncertainty in the absorption coefficient (8% relative) with the uncertainty in total absorbance, which was estimated individually for each sample as discussed in the appendix. Uncertainties in density were inconsequential when propagated and uncertainties in sample thickness were ignored. The resulting uncertainties range from 10-14%. We assumed the same relative uncertainties for concentrations calculated using the Libowitzky and Rossman (1997), for the sake of comparing calibration lines; the actual uncertainty when using this calibration is difficult to assess because the uncertainty in baseline varies depending on wavenumber.

SIMS

SIMS analyses were obtained on the Cameca 7f-GEO at the Center for Microanalysis at Caltech. We used a mass resolving power of ~5500 (M/ΔM), sufficient to separate the peaks for $^{16}O^{1}H$ and ^{19}F from ^{17}O and $^{18}O^{1}H$, respectively. For all analyses we collected 30 cycles through the mass sequence ^{12}C, $^{16}O^{1}H$, ^{18}O, ^{19}F, and ^{30}Si, measuring negative ions sputtered by a 5 nA Cs^{+} primary beam; other details concerning vacuum conditions, beam alignment, charge compensation, pre-sputtering, raster size, aperturing, and discrimination for surface contamination are outlined in Mosenfelder et al. (2011). Summaries of the data ($^{16}O^{1}H/^{30}Si$ and/or $^{19}F/^{30}Si$ ratios) are given for glasses in Table 2 and orthopyroxene and olivine in Table 4; errors are given as two times the standard deviation ($2\sigma_{\square\square}$) of 2-7 analyses per sample. We use ^{30}Si as the reference isotope throughout the rest of this paper but note that very similar trends and statistics

(internal precision, reproducibility, and relative slopes/goodness of fit to calibration data) apply when ^{18}O (which has a higher ion yield than ^{30}Si) is used instead. Complete data (count rates, ratios, and uncertainties for all reported masses, for individual analyses; uncertainties are given as two times the standard error ($2\sigma_{mean}$) of the 30 measurement cycles) are provided in the supplementary material. Although we only report analyses in this paper from a single analytical session conducted in April, 2012, isotopic ratios were consistent within ~10% with values measured on the same samples during the sessions reported in Mosenfelder et al. (2011).

Fluorine concentrations in NAMs were calibrated with reference to silicate glass standards (Table 2). For blank correction of the glass analyses we used synthetic forsterite GRR1017, a well-established blank standard for $^{16}O^{1}H$ that also yields low ^{19}F counts (Mosenfelder et al. 2011), around 30 cps (a low count rate considering the high ionization efficiency of ^{19}F compared to the other collected secondary ions). Although we cannot be certain that this sample gives a true blank measurement, we note that count rates are within error of each other (when measured sequentially) for GRR1017, synthetic orthopyroxene (see below), synthetic clinopyroxene (see part II), and synthetic zircon (unpublished data); this suggests that we are measuring the background due to F in the vacuum and/or memory effects (from deposition of F on the immersion lens), rather than F within the samples. We report F data for a total of 11 commonly used glass standards of varying composition (ranging from komatiitic to rhyolitic/high-Si synthetic glass), obtained from the United States Geological Survey (USGS), National Institute of Standards and Technology (NIST), and Max-Planck Institut (MPI-DING; Jochum et al. 2006). Table 2 lists F concentrations of the standards determined from selected previous

177 studies (Hoskin 1999; Straub and Layne 2003; Jochum et al. 2006; Guggino and Hervig
178 2010, 2011). The large variations in these values, combined with concerns about
179 heterogeneity in some glasses, prompt us to explore different models for F calibration, as
180 outlined in the results section.

181 Blank correction for $^{16}O^{1}H$ and ^{19}F in orthopyroxene was performed using OH-
182 poor and/or F-poor standards, which were measured periodically during the session to
183 monitor the background level. For this purpose we examined a synthetic enstatite
184 (GRR247, grown by Ito (1975) using flux methods) and a natural orthopyroxene that was
185 dehydrated in the lab (ZM1opx-HT) and compared them to GRR1017 forsterite.
186 ZM1opx-HT was dehydrated by heating under reducing conditions at 1000 °C for 72 h in
187 a one atmosphere Deltech^{TM} furnace, with oxygen fugacity controlled by a CO-CO_2 gas
188 mixture at $10^{-12.2}$ atm (corresponding to log f_{O2} approximately one order of magnitude
189 lower than the quartz-fayalite-magnetite buffer; cf. Aubaud et al. 2007). FTIR spectra
190 revealed no detectable OH, with a detection limit of approximately 1 ppm H_2O. On the
191 other hand, this sample retained relatively high (although variable) amounts of F, making
192 it unsuitable for that blank correction. Conversely, GRR247 was found to be unsuitable
193 for H correction but excellent for F correction. It contains a small amount of H_2O,
194 probably present as fluid inclusions (as evidenced by a weak broad IR band centered at
195 3400 cm^{-1} and reflected in measured $^{16}O^{1}H/^{30}Si$ ratios), but yielded very low ^{19}F counts
196 directly comparable to GRR1017 (~30 cps).

197 Estimated limits of detection (LOD) and quantitation (LOQ) for H, calculated
198 from analyses of ZM1opx-HT, regression of the data as detailed in the results section,
199 and the simple formulism of Long and Windefordner (1983) as used in Mosenfelder et al.

(2011) were 1 and 4 ppm H_2O, respectively. The LOD and LOQ for F (calculated in this case from analyses of GRR1017) are both less than 1 ppm regardless of which model for F calibration is used, ranging from 0.1 to 0.25 ppm (LOD) and 0.4 to 0.8 ppm (LOQ). These low values for F correspond well with estimated detection limits in previous studies, which also used synthetic forsterite to measure F backgrounds (Hauri et al. 2002; Jochum et al. 2006).

RESULTS

IR spectroscopy

Table 1 gives integrated absorbance for the three directions measured in each crystal. We also list absorbance for two wavenumber ranges ("low" versus "high"), separated by an arbitrary dividing line at 3350 cm^{-1} without performing any peak fitting to separate contributions of overlapping bands. IR spectra for all the samples (except the blank standards) are shown in Figure 1 in order of overall H concentration (Table 1). Note that the y-axis scales are different for each panel in the figure, where the scale for Figure 1c is compressed the most to show all the spectra together. Overall absorbance in most samples follows the order $\gamma > \alpha > \beta$, as observed in many other studies, but the degree of polarization varies greatly between samples (Table 1). The spectra show a wide range of band structures, with the number of different, strong peaks generally increasing with increasing H content. All samples show two or more bands between 3400 and 3560 cm^{-1}. However, the four mantle samples (KBH-1, DE2-1, PMR-54, and GKopxA), which have the highest H concentrations, show an additional band at ~3600 cm^{-1} in α and β (Fig. 1a,b) that is absent or greatly diminished in the other pyroxenes that are thought to

be crustal in origin. All samples also contain multiple bands in the range from ~3000-3400 cm^{-1}; the fine details of band structure in this region are difficult to see for all samples in Figure 1 due to scaling (for instance, compare the spectrum of KBH-1 in Figure 1c with the spectrum in Figure 2 of Bell et al. 1995).

We looked extensively for OH zoning in all of the pyroxenes, but found none with respect to the major bands shown in Figure 1. On the other hand, some crystals show variable amounts of absorbance at high wavenumbers (>3650 cm^{-1}) that we attribute to inclusions of hydrous phases. These bands were found in optically clear parts of the samples. Skogby et al. (1990) inferred the presence of amphibole and/or pyribole lamellae in many natural pyroxenes via comparison of sharp bands near 3675 cm^{-1} with corresponding bands in amphibole and pyribole spectra (Skogby and Rossman, 1991). Such "chain width defects", hereafter referred to for simplicity as amphibole lamellae, are also well known from TEM studies (e.g., Veblen 1985). In orthopyroxene, the amphibole lamellae IR bands are strongly polarized in the β direction (Skogby et al. 1990). In Figure 2 we show a comparison of spectra for some of our samples and spectra for hydrous phases from the literature. Bands clearly attributable to amphibole (note the comparison to pargasitic hornblende from Skogby and Rossman (1991)) were found in GRR2334a, JLM46, and JLM14, with average intensities increasing in that order. GRR1650b shows two sharper peaks at 3767 and 3760 cm^{-1} (Fig. 2), which could be from either tremolite or talc. The high wavenumber bands in GKopxA (Fig. 1b) are more difficult to interpret but we provisionally assign them to amphibole (these bands are also strongly polarized parallel to β). Finally, PMR-54 shows a complicated band structure with a peak at 3685 cm^{-1} that indicates the presence of serpentine, a common alteration product of

246 orthopyroxene (e.g., Gose et al. 2011). These bands are seen in both α (Fig. 2) and β
247 (Fig. 1) in this sample.

248 Hydrogen concentrations calculated using either the Bell et al. (1995) or
249 Libowitzky and Rossman (1997) calibrations are shown in Table 1. Note that the high
250 wavenumber bands associated with hydrous inclusions constitute less than 1% of the total
251 absorbance for all samples except JLM14 and were not included in the total absorbance
252 cited in Table 1. When we use the Libowitzky and Rossman calibration, calculated
253 concentrations are 3-14% lower for all samples except KBH-1 and PMR-54, for which
254 the calculated concentrations are higher (by 12% and 2%, respectively). There is a
255 systematic relationship (Fig. 3a) between the two calibrations as a consequence of the
256 differences in ratio of low to high wavenumber absorbance, which vary by up to a factor
257 of two among samples (using our arbitrary dividing line at 3350 cm^{-1}). Overall, however,
258 these subtle discrepancies balance out, leaving a strong, almost 1:1 correlation between
259 concentrations for all samples calculated using both calibrations (Fig. 3b). Similar trends
260 can be seen (Fig. 3b) for data on natural orthopyroxenes presented by Sundvall and
261 Stalder (2011). This result stands in strong contrast to the same exercise performed for
262 clinopyroxene, which shows a greater variation in mean wavenumber as we discuss in
263 Part II.

264

265 **SIMS: fluorine calibration**

266 In order to convert $^{19}F/^{30}Si$ ratios in NAMs to F, we calibrated using silicate
267 glasses with nominally well-determined F concentrations. For this purpose we multiplied
268 all ratios (both in standard glasses and in minerals) by SiO_2 content (Table 2). The

269 precision of our glass analyses was excellent, ranging from 0.3 to 0.9% ($2\sigma_{mean}$), but
270 reproducibility from 3-7 analyses of each standard varied between 1 and 11% (2σ□□).
271 Figure 4a shows our calibration curve for the MPI-DING and NIST glasses. Here we plot
272 F concentrations for MPI-DING samples as recommended by Jochum et al. (2006) based
273 on SIMS measurements conducted by Erik Hauri that are in turn referenced to EPMA
274 data on other standards (Hauri et al. 2002); for NIST standards we also plot the values
275 cited in Jochum et al. (2006). ATHO-G was excluded from this plot because its measured
276 $^{19}F/^{30}Si$ ratio (2.32) is wholly incompatible with the recommended value for F (0.7 ppm),
277 suggesting substantial heterogeneity in the glass. The data (including the blank standard,
278 GRR1017) were fit with both ordinary least-squares (OLS) and York (1966) regressions
279 and show a large degree of scatter that cannot be explained by the uncertainties of our
280 measurements alone.
281 Recently, Guggino and Hervig (2010, 2011) published considerably lower values
282 (compared to Jochum et al. 2006; see Table 2) for NIST SRM 610, NIST SRM 612,
283 ML3B-G, and KL2-G, as well as values for the USGS standard glasses BCR-2G, and
284 BHVO-2G. Their results for basalts (Guggino and Hervig 2011) are also tied to EPMA
285 data on other glasses (five basalts doped with between 0.2 and 2.5 wt% F), while their
286 values for NIST standards are based on proton induced gamma ray emission analyses
287 (Guggino and Hervig, 2010). We plot our data for these six standards against Guggino
288 and Hervig's values in Figure 4b, along with a York regression fitting only the basalt
289 data. Unfortunately, these points also show considerable scatter. As we discuss below, the
290 reasons for this are likely related more to heterogeneity in the glasses (e.g., due to F loss
291 during homogenization) than matrix effects; for instance, we could not reconcile the data

for the four basalts shown in Figure 4b by plotting against other chemical variables such as Mg/(Mg+Fe) ratio (cf. Figure 1d in Hauri et al. 2002), and the small variations in SiO_2 content also cannot explain the scatter.

Acknowledging the large degree of uncertainty in F measurements by SIMS implied by the above discussion, we use two different models to estimate F in NAMs in Table 4, based on either the Jochum et al. (2006) values or the Guggino and Hervig (2011) values for the standards (not including the NIST standards in the latter case). From simple inversion of the York regressions to the datasets shown in Figure 4 (which differ in slope by a factor of 2.14), we derive model 1 (based on Jochum et al. values):

$$F(ppm) = ({}^{19}F/{}^{30}Si \times SiO_2 + 0.031)/0.1241$$

and model 2 (based on Guggino and Hervig's data):

$$F(ppm) = ({}^{19}F/{}^{30}Si \times SiO_2 - 0.0004)/0.2654$$

where the ratios and SiO_2 values are taken from Tables 4 and 3, respectively.

SIMS: hydrogen and fluorine in orthopyroxene

Average measured ${}^{16}O^{1}H/{}^{30}Si$ ratios from 3-7 analyses for each sample are listed in Table 4. Typical internal precision for ${}^{16}O^{1}H/{}^{30}Si$ ratios was 1-3% ($2\sigma_{mean}$) for samples containing H, and 5-7% for ZM1opx-HT, the blank standard. Out of a total of 47 analyses, only three with much higher uncertainty were rejected based on the Poisson counting statistic criterion we used previously (Mosenfelder et al. 2011); these are not included in Table 4 but are given in the supplementary material. Reproducibility was 10% or better for most samples. However, JLM46 and JLM14 yielded more variable ${}^{16}O^{1}H/{}^{30}Si$ (spread by up to a factor of 2) despite high precision (i.e., flat depth profiles)

for individual analyses. This is illustrated in Figure 5, where we plot $^{16}O^{1}H/^{30}Si$ vs. $^{19}F/^{30}Si$ for selected samples. For the sake of illustration we also show an older analysis of JLM14 (from a session in 2010) that was even more discrepant with other analyses. There is a clear linear correlation ($r^2 = 0.999$) between ^{19}F and $^{16}O^{1}H$ for these two pyroxenes. According to IR spectra, as discussed above, they also contain the highest concentrations of amphibole lamellae. Because of the high probability that we ionized variable amounts of these lamellae, we culled the data by taking the analyses with the lowest measured $^{16}O^{1}H$ and ^{19}F as an upper constraint on the "true" value of amphibole-free orthopyroxene. This leaves three analyses (out of four) of JLM46 with $^{16}O^{1}H/^{30}Si$ = 0.0156±0.0001 and four analyses (out of seven) of JLM14 with $^{16}O^{1}H/^{30}Si$ = 0.0364±0.0034, which we used for the sake of the calibration lines presented next.

Figures 6a and 6b show the average measured $^{16}O^{1}H/^{30}Si$ ratios (normalized by multiplying by SiO_2 as determined by EPMA) plotted against concentrations determined from FTIR using the Bell et al. (1995) and Libowitzky and Rossman (1997) calibrations, respectively. Fits to the data (both OLS and York regressions) have virtually identical slopes and similar intercepts close to zero, despite the fact that H concentrations determined by the two IR calibrations vary significantly for some samples. To illustrate this last point in Figure 6b we use arrows to point to the two samples (KBH-1 and JLM14) whose H concentrations differ the most when applying the Libowitzky and Rossman (1997) calibration. Finally, we note the peculiarity that JLM14, the sample with the most amphibole lamellae, plots farthest from the best-fit line; ironically, if we use the average of all seven analyses listed in Table 4 for JLM14 it would plot exactly on the best-fit line shown in Figure 6a. In other words, this discrepancy is apparently not due to

338 measuring $^{16}O^{1}H$ in hydrous inclusions, a problem we assessed for olivine in
339 Mosenfelder et al. (2011).

340 Fluorine concentrations were calculated using the two different models for the
341 calibration on glasses; they range from 1 to 37 ppm for model 1, and 0.4 to 17 ppm for
342 model 2. In general, the orthopyroxenes from crustal environments (JLM50, JLM46,
343 GRR2334a, GRR1650b, and JLM14) have low amounts of F compared to mantle
344 samples, which have modest amounts. A single exception is GKopxA, which had the
345 lowest F of any natural orthopyroxene we measured, above the LOD but essentially at the
346 LOQ. In contrast to the recent study of Beyer et al. (2012) on a more limited set of
347 natural samples, we found no correlation between F and Al_2O_3 (Fig. 7). The lack of
348 correlation is not improved when F is compared to tetrahedral or octahedral Al (as
349 calculated from the EPMA data) or other trivalent cations (e.g., Cr^{3+}) are considered.
350

351 **SIMS: hydrogen and fluorine in olivine**

352 Figure 8 shows the olivine calibration conducted in the 2012 session. The level of
353 data scatter and quality of the regression are similar to previous calibrations (Mosenfelder
354 et al. 2011). We also show the same data for orthopyroxene as plotted in Figure 6a (i.e.,
355 assuming the Bell et al. calibration). The difference in slopes between the orthopyroxene
356 and olivine calibration lines is about 20%. This suggests a matrix effect between the two
357 phases that is not simply due to differences in ^{30}Si yield (because we normalized for
358 SiO_2). We evaluate this possibility further below, in the context of results from other
359 laboratories and the uncertainties in our regression analysis.

Using model 2 for the F calibration, F concentrations in olivine range from less than 1 ppm to about 50 ppm (or from 1 to 100 ppm for model 1). These values are ~27% lower than the preliminary values for the same samples that we presented in Mosenfelder et al. (2011). They are fairly consistent with recent studies (Guggino et al. 2007; Beyer et al. 2012), which examined a wider range of olivines. Much higher values were reported for Monastery olivines by Hervig and Bell (2005), obviously based on a different calibration. One sample (GRR1695-2) had low F but a very wide spread in $^{19}F/^{30}Si$, which we attribute to variable ionization of F-bearing nm-scale pores, as documented in Mosenfelder et al. (2011). Although we did not re-analyze some of the other olivines from Mosenfelder et al. (2011) in the session reported here, we can estimate their F concentrations by comparing previously measured $^{19}F/^{30}Si$ ratios among all the samples. The resulting values for KLV23, ROM250-OL2, and ROM250-OL13 are 6, 10, and 45 ppm respectively (assuming model 2).

DISCUSSION

Uncertainties in hydrogen measurements

Our study confirms previous work showing that low-blank, very high precision analyses (as good as 1% 2σ or even better) of trace H and F are attainable using SIMS. For H we depend on cross calibration with FTIR, which is subject to much larger uncertainties deriving from absorbance measurements and the calibration of the absorption coefficient. Unfortunately, these issues have not been resolved since being raised by Bell et al. (1995) and are treated in different ways in different studies.

In the present study, uncertainties due to differences in polarizer efficiency (Libowitzky and Rossman 1996) or imprecision in thickness or density measurements are inconsequential compared to the uncertainty in spectral baselines. Linear baselines, which have the obvious advantage of being inherently reproducible, are commonly used to correct spectra of synthetic enstatite (e.g., Stalder 2004; Prechtel and Stalder 2012). However, this type of correction is not appropriate for Fe-bearing orthopyroxene, because the baseline in this case is a complex, curved function of both Si-O vibrational bands and electronic transitions (Fe^{2+} in the M2 site, with bands at approximately 11000, 5400, and 2350 cm^{-1}; Goldman and Rossman 1976), with long tails of absorption. In the appendix we detail how we approached this problem.

Aside from uncertainties in absorption measurements, there is clearly further need for additional determinations of the IR absorption coefficient using absolute methods such as hydrogen manometry or nuclear microprobe techniques. An early attempt using NRA determined a value of 508 ppm H_2O for PMR-54 (unpublished work of R. Livi reported in Skogby et al. 1990). This is about twice as much as the value we infer for this pyroxene (Table 1) using either of the two IR calibrations. This analysis was obtained before the method was optimized and interferences with other nuclear reactions were recognized (Rossman 2006), and has been ignored in subsequent studies. However, it underscores the potential difficulties associated with achieving low blanks and/or discriminating against "contamination" by hydrous phase inclusions (in this case serpentine, as shown in Figure 2).

We have relied on the manometry calibration of Bell et al. (1995), who determined a value of 217±22 (2σ) ppm H_2O for KBH-1. Support for this value is given

405 by the more recent study of Wegdén et al. (2005), who measured 25 ppm H (equivalent to
406 223 ppm H_2O) in Kilbourne Hole orthopyroxene using proton-proton scattering. On the
407 other hand, O'Leary et al. (2007), employing continuous flow mass spectrometry,
408 measured a significantly lower H concentration in KBH-1. Their value of 165±40 ppm
409 H_2O (2σ) is only in weak agreement with Bell et al.'s value. Here we note that the
410 nominal value of 186 ppm H_2O cited in O'Leary et al. (2007), Bell and Ihinger (2000),
411 and Koga et al. (2003) represents only the amount of H_2O extracted for manometry, not
412 the original concentration, which Bell et al. (1995) calculated by estimating the amount
413 of O-H absorbance remaining in sample chips after extraction.
414 Variations like those shown in Figure 1 prompted Bell et al. (1995) to suggest that
415 the molar absorption coefficient probably varies among samples with different types of
416 spectra, making application of their calibration on KBH-1 to other pyroxenes non-ideal.
417 So far there has been only one attempt to conduct absolute calibrations on multiple
418 orthopyroxene samples with different IR spectra. Aubaud et al. (2009), using elastic
419 recoil detection analysis (ERDA), unfortunately concluded that the background H level of
420 the technique was too high to quantitatively determine absorption coefficients for the
421 samples they used (although it could be used in the same study for rhyolitic glasses and
422 synthetic olivines, with much higher H concentrations; in part II we also discuss their
423 results for clinopyroxene).
424
425 **Wavenumber-dependent, site-specific, or uniform IR absorption coefficients?**
426 The suggestion of Bell et al. (1995) that the molar absorption coefficient could
427 vary among samples with different spectra may have partially motivated subsequent

428 workers to prefer the Paterson (1982) or Libowitzky and Rossman (1997) calibrations,
429 which are both wavenumber dependent functions. The latter calibration has been used
430 especially frequently for pyroxenes (e.g., Stalder and Skogby 2002; Stalder 2004;
431 Nazzareni et al. 2011; Stalder et al. 2012), despite the fact that it was derived from fitting
432 data on stoichiometrically hydrous phases (whereas the Paterson calibration is primarily
433 based on various phases of water and water dissolved in organic solvents, glasses and
434 quartz). Support for a linear correlation between absorption coefficients and wavenumber
435 also comes from theoretical modeling of OH-containing molecules (Kubicki et al. 1993)
436 and hydrous phases (Balan et al. 2008). On the other hand, recent studies have argued
437 that these linear trends as a rule are inapplicable to NAMs (Rossman 2006; Thomas et al.
438 2009; Koch-Müller and Rhede 2010; Balan et al. 2011). It has also been proposed
439 (Kovács et al. 2010; Balan et al. 2011) that different O-H defect sites within a single
440 mineral can have absorption coefficients varying by much larger factors than those
441 predicted by any wavenumber-dependent calibration; this hypothesis was contested for
442 the case of olivine in our study using SIMS and FTIR (Mosenfelder et al 2011).
443 Our calibration for orthopyroxene (Fig. 6) shows that the data can be fit with the
444 same precision and indeed the same regression slope, within error, regardless of whether
445 a wavenumber-dependent or single absorption coefficient is used to calculate H contents
446 by FTIR; a similar conclusion is apparent from the data (see their Figure 9) of Aubaud et
447 al. (2007). Our samples show a wide range of band structures with variable percentages
448 of low- and high-wavenumber absorbance (Table 1, Fig. 3a). However, these differences
449 balance out as a result of the overall correlation between the two IR calibrations (Fig. 3b).
450 Therefore, we conclude that within the resolution of our methods it is not possible to

ascertain which calibration is more accurate. This result stands in contrast to our conclusion for SIMS data on clinopyroxenes, which can be fit better using a frequency dependent calibration as shown in Part II.

This assessment also contrasts with recent SIMS/FTIR work by Stalder et al. (2012), who studied pure (Fe- and Al-free) enstatites synthesized at 2.5-8 GPa that show variable absorbance for four major bands over a large wavenumber range (with band centers at 3090, 3360, 3590, and 3690 cm^{-1}). They concluded that applying different absorption coefficients to the four different bands was not meaningful, but that wavenumber dependent functions fit their data significantly better than using the single absorption coefficient of Bell et al. (1995). A similar conclusion was reached in an earlier study on synthetic clinopyroxenes (Stalder and Ludwig 2007). It should be emphasized that there are many differences between our studies, making straightforward comparison impossible. The SIMS technique used by Stalder et al. (2012) is novel for geological applications, relying on multiple analyses on the same spot at highly varying beam current to correct for the effects of high H background from contamination of the vacuum (Ludwig and Stalder 2007). These studies also rely on tourmaline standards for quantification, neglecting any possible matrix effects. Moreover, while three of the bands in the synthetic samples (3090, 3360, and 3590 cm^{-1}) are similar to bands seen in natural orthopyroxene, the fourth, at 3690 cm^{-1}, has not been encountered as a single sharp band in natural samples; bands at similar frequencies are interpreted to come from hydrous inclusions in natural samples (and are generally less intense) but are thought to represent structurally bound H in the experiments (Prechtel and Stalder 2012). This band contributes an outsized percentage to the total H calculated using the wavenumber

474 dependent calibration, by the very nature of the function. Thus it is not surprising that the
475 Bell et al. (1995) and Libowitzky and Rossman (1997) calibrations diverge strongly in
476 Figure 3 of Stalder et al. (2012). Therefore it is plausible that a wavenumber dependent
477 function is superior for synthetic high-pressure enstatites, but not justified for natural
478 orthopyroxenes.
479
480 **SIMS: matrix effects**
481 One of the most important concerns with using SIMS to measure H in NAMs is
482 the magnitude of matrix effects, which have been addressed in some studies and ignored
483 in others. Koga et al. (2003) and Aubaud et al. (2007) documented differences in
484 calibration slopes among different NAM, hydrous minerals, and silicate glasses up to a
485 factor of 4.25. Other studies have neglected matrix effects entirely, yet recommended
486 new absorption coefficients for NAMs based on calibration tied to different minerals. In
487 the case of orthopyroxene, Stalder et al. (2005, 2012) suggested that existing IR
488 calibrations systematically underestimate H (by a factor of 1.4. to 1.7). However, the use
489 of tourmaline as the standard for their SIMS analyses makes this conclusion tenuous until
490 the magnitude of matrix effects can be established.
491 Koga et al. (2003) postulated that the matrix effect between olivine and
492 orthopyroxene should be minimal, based on the similarity in mean atomic weight and
493 chemistry between these minerals. Although they successfully regressed their olivine and
494 orthopyroxene SIMS data together, the H concentrations in most of their orthopyroxenes
495 were imprecisely determined based on adjusting (by a factor of 2) concentrations
496 determined using the Paterson (1982) calibration on unpolarized spectra. Moreover, they

497 did not correct their data for the differences in SiO_2 content, as we have done here
498 following typical protocol for evaluating matrix effects (e.g., Hinthorne and Andersen
499 1975; Ihinger et al. 1994; Aubaud et al. 2007). If their data are normalized in this way, a
500 difference between the calibrations for olivine and orthopyroxene emerges that is similar
501 to the later results of Aubaud et al. (2007), who used the same IR calibrations we have
502 used here to establish a factor of 1.5 difference in calibration slopes for the two phases. A
503 similar difference (factor of 1.4) can be seen in calibration slopes later measured for the
504 same standards by Tenner et al. (2009) using analytical conditions similar to those we
505 used, in particular measuring $^{16}O^{1}H$ rather than ^{1}H. However, the H concentrations of
506 many of the synthetic olivines used in earlier studies were subsequently revised by
507 Withers et al. (2011), who then found indistinguishable calibration slopes for olivine and
508 orthopyroxene. Another possibility to consider is that there may be a fundamental
509 difference in the effect of the matrix on yield of lighter ^{1}H ions (as measured in the earlier
510 studies) versus $^{16}O^{1}H$.

511 Our calibration slopes (Fig. 8) for orthopyroxene and olivine, acquired in the
512 same session, are within about 20% of each other. This reinforces the idea that the matrix
513 effect between these two minerals is small. Furthermore, the difference may be even less
514 if more recent values for the IR absorption coefficient for olivine are considered. Thomas
515 et al. (2009) derived a range of ε_i values between ~28000-47000 l mol^{-1}_{H2O} cm^{-2} for
516 olivines with different spectral characteristics, based on two different techniques (proton-
517 proton scattering and Raman spectroscopy). More recently, using ERDA, Withers et al.
518 (2012) derived an ε_i of 45,200 l mol^{-1}_{H2O} cm^{-2} for olivine. Use of the higher values would

519 result in lower amounts of H in olivine, thereby bringing the two calibration lines closer
520 together (in fact, crossing over each other in our particular case).

521 Matrix effects have also been well documented for solid solution within single
522 mineral groups, but the mechanisms responsible for the effects are still unclear. For
523 instance, Ottolini et al. (2002) showed that H yields decrease with increasing Fe+Mn in a
524 variety of hydrous minerals such as kornerupine, tourmaline, and micas, when using a
525 $^{16}O^-$ primary beam and an energy-filtered secondary ion beam. In an earlier paper
526 (Ottolini and Hawthorne 2001) it was speculated that this effect might be due to
527 oxidation-dehydrogenation reactions (buffered by implantation of oxygen from the
528 primary beam), resulting in liberation of a neutral species (H_2O or H_2) that goes
529 undetected in the mass spectrometer. This effect cannot be relevant in our study, which
530 used a Cs^+ beam (and no energy filtering); indeed, data from Koga et al. (2003) suggest
531 the reverse phenomenon, with H/Si generally increasing with increasing Fe. Moreover,
532 oxidation cannot easily explain the fact that yields of other lights elements (Li, B, and F)
533 also decrease with increasing Fe+Mn. More likely, the matrix effect is related to an
534 overall increase in molecular weight of the matrix, which has generally been shown to
535 decrease H/Si ratios (King et al. 2002) as well as fractionate D/H to higher values (Hauri
536 et al. 2006b); in the former case it is unclear whether H yields go down or Si yields go
537 up. Our data are very limited in this respect but suggest that orthopyroxenes with Mg
538 numbers (100 × molar Mg/(Mg+Fe); Table 3) between 79 (GRR1650b) and 99 (JLM50)
539 show no statistically meaningful Fe-related matrix effect for H; a similar conclusion was
540 reached for garnets of varying Mg number by Aubaud et al. (2007). Nevertheless, future
541 work to explore the effect of Fe on H yield is warranted in order to better quantify H in

Fe-rich NAMs from Martian and lunar rocks (e.g., Boctor et al. 2003; Liu et al. 2012) as well as experimental samples with high Fe (and considerably more H compared to natural samples) designed to model the Martian mantle (Withers et al. 2011).

SIMS: analysis of hydrous inclusions

A general problem for SIMS measurements of H in NAMs is the possibility of ionizing fluid inclusions or inclusions of hydrous phases. Aubaud et al. (2007) inferred that SIMS could be more effective than FTIR at screening out contributions from H that is not bound in lattice defects, because of its very limited sampling volume compared to FTIR. On the contrary, in Mosenfelder et al. (2011) we emphasized that ionization of hydrous inclusions can result in severely skewed OH/Si ratios, depending on the volume of nanometer- to micron-scale inclusions that are sampled. This stochastic phenomenon is also seen here for those samples containing relatively high abundances of amphibole lamellae (JLM46 and JLM14), a common features in many pyroxenes (Skogby et al. 1990). However, there is a significant difference between the results on orthopyroxene and olivine. In the latter case we found that "contaminated" analyses can usually be easily identified by considering the ratio of the standard error of the mean to the error predicted by Poisson counting statistics ($\sigma_{mean}/\sigma_{Poisson}$). For olivine, we used a cut-off criterion, filtering analyses with $\sigma_{mean}/\sigma_{Poisson} > 5$. For orthopyroxene, most of our analyses are highly precise with $\sigma_{mean}/\sigma_{Poisson}$ close to 1, even when we infer that amphibole lamellae have been sampled. Our filtering criterion in this case is based on comparison of $^{16}O^{1}H/^{30}Si$ and $^{19}F/^{30}Si$ ratios (Fig. 5), making the simplistic assumption that both H and F partition strongly into amphibole. The different behavior for pyroxene analyses

565 presumably reflects differences in the geometrical relationship of the host phase to
566 inclusions; the lamellae may form in wide (but thin) layers that are evenly sampled
567 during sputtering, while the sub-micron scale, ovoid fluid inclusions we imaged in
568 olivines may have a very heterogeneous distribution even on the small scale of a SIMS
569 analysis pit. A similar phenomenon could be envisaged for Ti-clinohumite lamellae or
570 platelets in olivine (Mosenfelder et al. 2006b). An important corollary of this result is that
571 SIMS studies of natural pyroxenes should probably be accompanied by at least
572 qualitative FTIR spectroscopy (e.g., unpolarized spectra taken through polycrystalline
573 samples), because the presence of hydrous inclusions may not be easy to determine by
574 SIMS alone and is also sometimes difficult to detect using optical microscopy.
575

576 **Uncertainties in fluorine measurements**

577 As there are no well-established matrix-matched standards for F in NAMs, we
578 took the same approach as other workers (Hervig and Bell 2005; Hauri et al. 2006a;
579 Guggino et al. 2007; O'Leary et al. 2010; Dalou et al. 2012) of using F-bearing silicate
580 glasses for calibration. Two other recent studies (Bernini et al. 2012; Beyer et al. 2012)
581 have taken a fundamentally different approach of using ion implanted natural forsterite
582 and enstatite crystals for standardization. Unfortunately, the large variation in regression
583 slopes and high uncertainty envelopes for the different models shown in Figure 4
584 underscore the large uncertainty in using silicate glasses for F calibration. Possible
585 factors contributing to this uncertainty include: fundamental errors in determinations of
586 the standards; heterogeneity in the standards; matrix effects due to chemistry within the

587 glasses themselves; and matrix effects resulting from the difference in structure between
588 amorphous and crystalline materials.

589 The large discrepancies in values determined for F in the MPI-DING glasses by
590 Jochum et al. (2006) and Guggino and Hervig (2011) are as yet unexplained but could be
591 related to either or both of the first two issues mentioned above. In both cases F was
592 determined by calibration on other glasses with concentrations high enough to measure
593 by EPMA, a notoriously difficult analytical method to use for F due to problems
594 including low X-ray peak intensity, volatile migration, and interferences by higher order
595 peaks from transition elements, particularly Fe$L\alpha_1$ (for more detailed discussion see
596 Witter and Kuehner 2004). In this respect we presume that the more recent results of
597 Guggino and Hervig (2011) are more reliable because they used multiple synthetic F-
598 bearing glasses as standards and employed peak-integration analysis rather than using
599 peak heights, a more typical method for reducing EPMA data. We note that using this
600 calibration gives a lower value for F in Monastery olivines (e.g., 37 ppm in ROM177,
601 compared to 80 ppm for model 1) that is more consistent with the measurement of 30
602 ppm F in a Monastery olivine by Beyer et al. (2012).

603 Even assuming that Guggino and Hervig's values for basalts are correct, we still
604 have considerable scatter in our calibration (Fig. 4b). One concern with glasses, which
605 has been particularly well documented for the NIST samples (Hoskin 1999; Eggins and
606 Shelley 2002), is that volatile elements (purposely-doped in the case of NIST) can be lost
607 during fabrication, for instance escaping along "cord structures" that form during melting.
608 We were unable to locate cord structures in our NIST standards using optical methods
609 (Eggins and Shelley 2002) and elected to just cut small slabs from the middle of the as-

610 provided wafers, the region least likely to have suffered from volatile loss. As for the
611 MPI-DING and USGS glasses, more work is clearly needed to establish levels of
612 homogeneity. The loss of other elements besides F has been documented in some of the
613 MPI-DING glasses. For instance, Borisova et al. (2010) found significant depletion of
614 many elements in ATHO-G in an anomalous split, and attributed the discrepancy either to
615 loss to the crucible wall or development of compositional cords. This could easily explain
616 the severe discrepancy between our measured ^{19}F yield for ATHO-G and the much lower
617 reference value from Jochum et al. (2006), as well as scatter among the other glasses we
618 used.

619 The extent to which matrix effects are important for F in glasses has yet to be
620 elucidated and is the subject of ongoing studies (Rose-Koga et al. 2008; Guggino and
621 Hervig 2010, 2011). Although these effects might be expected to be very small as a result
622 of the high ionization efficiency of F (Williams 1992), Guggino and Hervig (2011)
623 estimate matrix effects of ~50% between low- and high-silica glasses. This difference is
624 much larger than a previous estimate of 15% from the same lab for a range of phases
625 (Jamtveit and Hervig 1994). Sensible trends in this regard are difficult to decipher from
626 the data shown in Figure 4a not only because of data scatter, but because the F in the
627 standards was established in the first place under the assumption that matrix effects are
628 small – within the assigned, overall uncertainties (precision and accuracy) of 10%
629 (Jochum et al. 2006). As for possible differences in ion yield due to the fundamental
630 structural differences between amorphous glasses and the crystalline silicates of primary
631 interest to use here, there are very few constraints currently, but we would point out that
632 differences in H yield can be quite large between silicate glasses and NAMs (Koga et al.

633 2003; Aubaud et al. 2007). All of these issues point to the need in future studies to
634 establish matrix-matched standards for NAMs, perhaps by synthesis at high pressures and
635 temperatures or by ion implantation (Bernini et al. 2012; Beyer et al. 2012).
636
637 **Fluorine in nominally fluorine-free minerals**
638 Fluorine is readily incorporated in the same sites as OH in hydrous minerals such
639 as amphiboles, micas, and the humite-series, as well as in apatite. Analyses of these
640 phases form the basis for classic studies of F distribution within the crust and mantle
641 (Aoki and Kanisawa 1979; Aoki et al. 1981; Smith et al. 1981; Edgar et al. 1996). One of
642 the implicit and explicit (Smith et al. 1981) assumptions of this work is that the common
643 upper mantle NAMs (olivine, garnet, ortho- and clinopyroxene) do not contribute
644 significantly to the bulk F content of the mantle. A very similar view was held about H
645 until increasing evidence was provided from IR studies that contradicted this idea (e.g.,
646 Aines and Rossman 1984; Bell et al. 1992).
647 The F concentrations we measured for olivine and orthopyroxene are indeed quite
648 low (less than ~50 ppm) compared to F in phases such as phlogopite or amphibole from
649 the studies mentioned above. However, when considered in the context of modal
650 abundance, these amounts may be more than sufficient to account for the inferred F
651 budget of the mantle (Beyer et al. 2012). In general, we found that F is much lower in
652 crustal-derived orthopyroxene and olivine, compared to mantle samples; importantly, we
653 can rule out the presence of amphibole (which might preferentially partition F) in the
654 latter pyroxenes because IR is very sensitive to small concentrations of lamellae (Skogby
655 et al. 1990). However, we see a distinct trend of higher F in megacrysts from South

656 African kimberlites (PMR-54 and DE2-1 orthopyroxene; Monastery olivines) compared
657 to xenocrysts from minette diatremes in the Colorado Plateau (GKopxA orthopyroxene;
658 GRR1629-2 and GRR1784e olivine). For the Monastery kimberlite, we also confirm the
659 distinct difference depending on petrologic context that was reported by Hervig and Bell
660 (2005): F is lower in group 1 or "main silicate trend" olivine (ROM250-OL2) compared
661 to Fe-rich "group 2" olivines (ROM177 and ROM250-OL13). These results imply that
662 different mantle reservoirs have different amounts of F (possibly related to the degree of
663 differentiation in the Monastery samples), and that F is not necessarily correlated with
664 other volatile concentrations (H concentrations are inferred to be high in the mantle
665 below both the Colorado Plateau and South Africa). Beyer et al. (2012) reached a
666 different conclusion, inferring similar amounts of F in different mantle reservoirs based
667 on measurements in natural olivines (nine samples) and orthopyroxenes (three samples)
668 from different localities. Of course, both of our limited surveys have unavoidable
669 sampling bias. For instance, we would not be surprised to see much higher F in
670 orthopyroxenes associated with F-rich phlogopite from ultra-high temperature granulite
671 terranes (Motoyoshi and Hensen 2001), or in highly metasomatized mantle xenoliths such
672 as those from West Eifel, Germany (Edgar et al. 1996). Moreover, Beyer et al. (2012)
673 only studied one olivine derived from the garnet-lherzolite facies, so their inference of
674 homogeneity among mantle reservoirs only reasonably applies to the upper-most mantle
675 (plagioclase- and spinel-lherzolite facies).

676 Experimental studies have shown that NAMs can incorporate approximately an
677 order of magnitude more H – at very high pressures – than their most hydrous
678 counterparts found so far in nature. By the same token, it is not surprising to see that

679 experimental studies are finding the same phenomenon for F. Several recent experimental
680 studies bear on this topic, although the wide pressure range that has been examined for
681 NAMs has yet to be fully explored for studies of F. In Fe-free systems at moderate
682 pressures (1-2.6 GPa), Bromiley and Kohn (2007) and Bernini et al. (2012) measured up
683 to 4500 ppm and 1900 ppm F respectively, in forsterite; the latter study also documents
684 up to 336 ppm F in enstatite and 1110 ppm F in pyrope. In more complex systems, Hauri
685 et al. (2006a) and O'Leary et al. (2010) measured F, Cl, S, and H in NAMs equilibrated
686 with basaltic melts from 0.5-4 GPa and 1000-1370 °C under water-saturated conditions.
687 While the focus of these two studies was on H partitioning, they measured up to 13, 16,
688 88, and 138 ppm F in olivine, garnet, orthopyroxene, and clinopyroxene, respectively.
689 Hauri et al. (2006a) also found that orthopyroxene/melt partition coefficients for F ($D_F^{opx-melt}$)
690 were about twice as high (ranging from 0.015 to 0.0448) as those for H. More recent
691 experiments by Dalou et al. (2012) and Beyer et al. (2012) were conducted at similar
692 pressures and temperatures, but under nominally anhydrous conditions and with
693 deliberately doped, higher amounts of halogens as in the studies in Fe-free systems.
694 Consequently, F contents of orthopyroxene in some of these experiments are much higher
695 (up to 432 and 571 ppm measured by Beyer et al. and Dalou et al., respectively). Dalou et
696 al. (2012) ascribed a very large variation of $D_F^{opx-melt}$ (0.0158-0.1841) in their
697 experiments to a dependence on the calculated viscosities of the investigated melts, while
698 Beyer et al. (2012) measured a much more restricted range of partition coefficients
699 ($D_F^{opx-melt}$ = 0.031-0.037). Beyer et al. (2012) also documented a correlation between Al
700 and F in both natural and synthetic orthopyroxenes that was not seen by Dalou et al.
701 (2012) and is not seen in the natural samples from the present study (Fig. 7),

underscoring the need for further work to assess the incorporation mechanisms for F in orthopyroxenes as well as other NAMs.

Although there are discrepancies between these experimental results that remain to be rectified, when considered together they indicate that F is a much more compatible element in NAMs than H. One consistency between the studies of Hauri et al. (2006a) and Dalou et al. (2012) is that they both found that the compatibility of F on average followed the order of clinopyroxene > orthopyroxene > garnet > olivine. This result contrasts with our results on natural mantle-derived NAMs, where overall we find the highest F contents in clinopyroxene (part II of this study), followed by olivine, orthopyroxene, garnet, and zircon (unpublished data for the latter two phases). Clearly more work is needed on both ends, to systematically explore the thermodynamics of F incorporation in experiments while documenting coexisting phases in xenoliths, which we have not done here, to gain better constraints on F partitioning behavior.

ACKNOWLEDGMENTS

We acknowledge funding to GRR from NSF grant EAR-0947956 and the White Rose Foundation. The Caltech center for Microanalysis, partially supported by the Gordon and Betty Moore foundation, also provided some support for the SIMS analyses. We thank Yunbin Guan for assistance with the ion microprobe, Chi Ma for assistance with the electron microprobe, and John Beckett for assistance with the gas-mixing 1-atm furnace. Zachary Morgan donated the mineral separate used to make the ZM1opx-HT sample, and David Bell has kindly allowed continued use of samples from his dissertation work at Caltech. Discussions with Richard Hervig and Marion Le Voyer on the topic of

fluorine measurements were enlightening and encouraging. Finally, we thank the associate editor (Roland Stalder) and an anonymous reviewer for their comments that helped greatly to clarify the manuscript.

REFERENCES

Aines, R.D. and Rossman, G.R. (1984) Water in minerals? A peak in the infrared. Journal of Geophysical Research, 89, 4059-4071.

Aoki, K. and Kanisawa, S. (1979) Fluorine contents of some hydrous minerals derived from upper mantle and lower crust. Lithos, 12, 167-171.

Aoki, K., Ishikawa, K., and Kanisawa, S. (1981) Fluorine geochemistry of basaltic rocks from continental and oceanic regions and petrogenetic appplication. Contributions to Mineralogy and Petrology, 76, 53-59.

Asimow, P.D., Stein, L.C., Mosenfelder, J.L., and Rossman, G.R. (2006) Quantitative polarized FTIR analysis of trace OH in populations of randomly oriented mineral grains. American Mineralogist, 91, 278-294.

Aubaud, C., Withers, A.C., Hirschmann, M., Guan, Y., Leshin, L.A., Mackwell, S., and Bell, D.R. (2007) Intercalibration of FTIR and SIMS for hydrogen measurements in glasses and nominally anhydrous minerals. American Mineralogist, 92, 811-828.

Aubaud, C., Bureau, H., Raepsaet, C., Khodja, H., Withers, A.C., Hirschmann, M.M., and Bell, D.R. (2009) Calibration of the infrared molar absorption coefficients for H in olivine, clinopyroxene and rhyolitic glass by elastic recoil detection analysis. Chemical Geology, 262, 78-86.

748 Balan, E., Refson, K., Blanchard, M., Delattre, S., Lazzeri, M., Ingrin, J., Mauri, F.,
749 Wright, K., and Winkler, B. (2008) Theoretical infrared absorption coefficient of
750 OH groups in minerals. American Mineralogist, 93, 950-953.
751 Balan, E., Ingrin, J., Delattre, S., Kovács, I., and Blanchard, M. (2011) Theoretical
752 infrared spectrum of OH-defects in forsterite. European Journal of Mineralogy,
753 23, 285-292.
754 Bell, D.R. and Ihinger, P.D. (2000) The isotopic composition of hydrogen in nominally
755 anhydrous mantle minerals. Geochimica et Cosmochimica Acta, 64, 2109-2118.
756 Bell, D.R. and Rossman, G.R. (1992) Water in the Earth's mantle: the role of nominally
757 anhydrous minerals. Science, 255, 1391-1397.
758 Bell, D.R., Ihinger, P.D., and Rossman, G.R. (1995) Quantitative analysis of trace OH in
759 garnet and pyroxenes. American Mineralogist, 80, 465-474.
760 Beran, A. and Zemann, J. (1986) The pleochroism of a gem-quality enstatite in the region
761 of the OH stretching frequency, with stereochemical interpretation. Tschermaks
762 Mineralogische und Petrographische Mitteilungen, 35, 19-25.
763 Bernini, D., Wiedenbeck, M., Dolejs, D., and Keppler, H. (2012) Partitioning of halogens
764 between mantle minerals and aqueous fluids: implications for the fluid flow
765 regime in subduction zones. Contributions to Mineralogy and Petrology,
766 doi:10.1007/s00410-012-0799-4.
767 Beyer, C., Klemme, S., Wiedenbeck, M., Stracke, A., and Vollmer, C. (2012) Fluorine in
768 nominally fluorine-free mantle minerals: experimental partitioning of F between
769 olivine, orthopyroxene, and silicate melts with implications for magmatic
770 processes. Earth and Planetary Sciences, 337-338, 1-9.

Boctor, N.Z., Alexander, C.M. O'D, Wang, J., and Hauri, E. (2003) The sources of water in the Martian meteorites: clues from hydrogen isotopes. Geochimica et Cosmochimica Acta, 67, 3971-3989.

Borisova, A.Y., Freydier, R., Polvé, M., Jochum, K.P., and Candaudap, F. (2010) Multi-elemental analysis of ATHO-G rhyolitic glass (MPI-DING reference material) by femtosecond and nanosecond LA-ICP-MS: evidence for significant heterogeneity of B, V, Zn, Mo, Sn, Sb, Cs, W, Pt and Pb at the millimetre scale. Geostandards and Geoanalytical Research, 34, 245-255.

Bromiley, D.W. and Kohn, S.C. (2007) Comparisons between fluoride and hydroxide incorporation in nominally anhydrous and fluorine-free mantle minerals. Geochimica et Cosmochimica Acta, 71, Goldschmidt Conference Abstracts, A124.

Dalou, C., Koga, K.T., Shimizu, N., Boulon, J., and Devidal, J.L. (2012) Experimental determination of F and Cl partitioning between lherzolite and basaltic melt. Contributions to Mineralogy and Petrology, DOI 10.1007/s00410-011-0688-2.

Edgar, A.D., Pizzolato, L.A., and Sheen, J. (1996) Fluorine in igneous rocks and minerals with emphasis on ultrapotassic mafic and ultramafic magmas and their mantle source regions. Mineralogical Magazine, 60, 243-257.

Eggins, S.M. and Shelley, J.M.G. (2002) Compositional heterogeneity in NIST SRM 610-617 glasses. Geostandards Newsletter, 26, 269-286.

Goldman, D.S. and Rossman, G.R. (1976) Identification of a mid-infrared electronic absorption band of Fe^{2+} in the distorted M(2) site of orthopyroxene, $(Mg,Fe)SiO_3$. Chemical Physics Letters, 41(3), 474-475.

794 Gose, J., Schmädicke, E., and Beran, A. (2009) Water in enstatite from Mid-Atlantic
795 ridge peridotite: evidence for the water content of suboceanic mantle? Geology,
796 37, 543-546.
797 Gose, J., Schmädicke, E., and Stalder, R. (2011) Water in mantle orthopyroxene - no
798 visible change in defect water during serpentinization. European Journal of
799 Mineralogy, 23, 529-536.
800 Guggino, S.N. and Hervig (2010) Determination of fluorine in fourteen microanalytical
801 geologic reference materials using SIMS, EPMA, and proton induced gamma ray
802 emission (PIGE) analysis. American Geophysical Union, Fall Meeting 2010,
803 abstract #V51C-2209.
804 Guggino, S.N. and Hervig, R.L. (2011) Synthesis and characterization of five new F-
805 bearing basalt reference materials (Fba glasses): quantifying the fluorine content
806 of the basaltic glass standards BCR-2G, BHVO-2G, GSA-1G, GSC-1G, GSD-1G,
807 GSE-1G, ML3B-G, KL2-G, and ALV-519-4. American Geophysical Union, Fall
808 Meeting 2011, abstract #V31C-2535.
809 Guggino. S.N., Hervig, R.L., and Bell, D.R. (2007) Fluorine in olivine from plutonic,
810 extrusive, and hypabbysal suites. American Geophysical Union, Fall Meeting
811 2007, abstract #V41B-0609.
812 Hålenius, U., Skogby, H., Edén, M., Nazzareni, S., Kristiannson, P., and Resmark, J.
813 (2010) Coordination of boron in nominally boron-free rock forming silicates:
814 evidence for incorporation of BO_3 groups in clinopyroxene. Geochimica et
815 Cosmochimica Acta, 74, 5672-5679.

816 Hauri, E.H., Wang, J., Dixon, J.E.,, King, P.L., Mandeville, C., and Newman, S. (2002)
817 SIMS analysis of volatiles in silicate glasses 1. Calibration, matrix effects and
818 comparisons with FTIR. Chemical Geology, 183, 99-114.
819 Hauri, E.H., Gaetani, G.A., and Green, T.H. (2006a) Partitioning of water during melting
820 of the Earth's upper mantle at H_2O-undersaturated conditions. Earth and Planetary
821 Science Letters, 248, 715-734.
822 Hauri, E.H., Shaw, A.M., Wang, J., Dixon, J.E., King, P.L., and Mandeville, C. (2006b)
823 Matrix effects in hydrogen isotope analysis of silicate glasses by SIMS. Chemical
824 Geology, 235, 352-365.
825 Hervig, R.L. and Bell, D.R. (2005) Fluorine and hydrogen in mantle megacrysts.
826 American Geophysical Union, Fall Meeting 2005, abstract #V41A-1426.
827 Hinthorne, J.R. and Andersen, C.A. (1975) Microanalysis for fluorine and hydrogen in
828 silicates using the ion microprobe mass analyzer. American Mineralogist, 60,
829 143-147.
830 Hoskin, P.W.O. (1999) SIMS determination of μg g^{-1}-level fluorine in geological samples
831 and its concentration in NIST SRM 610. Geostandards Newsletter, 23, 69-76.
832 Ihinger, P.D., Hervig, R.L., and McMillan, P.F. (1994) Analytical methods for volatiles
833 in glasses. In M.R. Carroll and J. R. Holloway, Eds., Volatiles in Magmas, 30, p.
834 67-121. Reviews in Mineralogy, Mineralogical Society of America. Chantilly,
835 Virginia.
836 Ito, J. (1975) High temperature solvent growth of orthoenstatite, $MgSiO_3$, in air.
837 Geophysical Research Letters, 2, 533-536.

838 Jamtveit, B. and Hervig, R.L. (1994) Constraints on transport and kinetics in
839 hydrothermal systems from zoned garnet crystals. Science, 263, 5050-508.
840 Jochum, K.P., Stoll, B., Herwig, K., Willbold, M., Hofmann, A.W., Amini, M., Aarburg,
841 S., Abouchami, W., Hellebrand, E., Mocek, B., and others (2006) MPI-DING
842 reference glasses for in situ microanalysis: new reference values for element
843 concentrations and isotope ratios. Geochemistry, Geophysics, and Geosystems, 7,
844 doi: 10.1029/2005GC001060.
845 King, P.L., Venneman, T.W., Holloway, J.R., Hervig, R.L., Lowenstern, J.B., and
846 Forneris, J.F. (2002) Analytical techniques for volatiles: a case study using
847 intermediate (andesitic) glasses. American Mineralogist, 87, 1077-1089.
848 Koch-Müller, M. and Rhede, D. (2010) IR absorption coefficients for water in nominally
849 anhydrous high-pressure minerals. American Mineralogist, 95, 770-775.
850 Koga, K., Hauri, E., Hirschmann, M.M., and Bell, D. (2003) Hydrogen concentration
851 analyses using SIMS and FTIR: comparison and calibration for nominally
852 anhydrous minerals. Geochemistry, Geophysics, and Geosystems, 4, doi:
853 10.1029/2002GC000378.
854 Kohlstedt, D. L., H. Keppler, and D. C. Rubie (1996), Solubility of water in the α, β, and
855 γ phases of $(Mg, Fe)_2SiO_4$. Contributions to Mineralogy and Petrology, 123, 345-
856 357.
857 Kovács, I., O'Neill, H.S.C., Hermann, J., and Hauri, E.H. (2010) Site-specific infrared O-
858 H absorption coefficients for water substitution into olivine. American
859 Mineralogist, 95, 292-299.

Kubicki, J.D., Sykes, D., and Rossman, G.R. (1993) Calculated trends of OH stretching vibrations with composition and structure in aluminosilicate molecules. Physics and Chemistry of Minerals, 20, 425-432.

Kurosawa, M., Yurimoto, H., and Sueno, S. (1997) Patterns in the hydrogen and trace element compositions of mantle olivines. Physics and Chemistry of Minerals, 24, 385-395.

Lemaire, C., Kohn, S.C., and Brooker, R.A. (2004) The effect of silica activity on the incorporation mechanisms of water in synthetic forsterite: a polarised infrared spectroscopic study. Contributions to Mineralogy and Petrology, 147, 48-57.

Libowitzky, E. and Rossman, G.R. (1996) Principles of quantitative absorption measurements in anisotropic crystals. Physics and Chemistry of Minerals, 23, 319-327.

Libowitzky, E. and Rossman, G.R. (1997) An IR absorption calibration for water in minerals. American Mineralogist, 82, 1111-1115.

Liu, Y., Mosenfelder, J.L., Guan, Y., Rossman, G.R., Eiler, J.M., and Taylor, L.A. (2012) SIMS analysis of water abundance in nominally anhydrous minerals in lunar basalts. 43rd Lunar and Planetary Science Conference abstract 1866.

Long, G.L. and Windefordner, J.D. (1983) Limit of detection. A closer look at the IUPAC definition. Analytical Chemistry, 55, 712A-724A.

Ludwig, T. and Stalder, R. (2007) A new method to eliminate the influence of *in situ* contamination in SIMS analysis of hydrogen. Journal of Analytical Atomic Spectrometry, 22, 1415-1419.

Mierdel, K. and Keppler, H. (2004) The temperature dependence of water solubility in enstatite. Contributions to Mineralogy and Petrology, 148, 305-311.

Mierdel, K., Keppler, H., Smyth, J.R., and Langenhorst, F. (2007) Water solubility in aluminous orthopyroxene and the origin of Earth's asthenosphere. Science, 315, 364-368.

Miller, G.H., Rossman, G.R., and Harlow, G.E. (1987) The natural occurrence of hydroxide in olivine. Physics and Chemistry of Minerals, 14, 461-472.

Mitchell, R.H. (1987) Megacrysts in kimberlites from the Gibeon field, Namibia. Neues Jahrbuch für Mineralogie Abhandlungen, 157, 267-283.

Mosenfelder, J.L., Deligne, N.I., Asimow, P.D., and Rossman, G.R. (2006a) Hydrogen incorporation in olivine from 2-12 GPa. American Mineralogist, 91, 285-294.

Mosenfelder, J.L., Sharp, T.G., Asimow, P.D., and Rossman, G.R. (2006b) Hydrogen incorporation in natural mantle olivines In S.D. Jacobsen and S. van der Lee, Eds., Earth's Deep Water Cycle p. 45-56. American Geophysical Union, Washington, D.C.

Mosenfelder, J.L., Le Voyer, M., Rossman, G.R., Guan, Y., Bell, D.R., Asimow, P.D., and Eiler, J.M. (2011) Analysis of hydrogen in olivine by SIMS: evaluation of standards and protocol. American Mineralogist, 96, 1725-1741.

Motoyoshi, Y. and Hensen, B.J. (2001) F-rich phlogopite stability in ultra-high-temperature metapelites from the Napier Complex, East Antarctica. American Mineralogist, 86, 1404-1413.

Nazzareni, S., Skogby, H., and Zanazzi, P.F. (2011) Hydrogen content in clinopyroxene phenocrysts from Salina mafic lavas (Aeolian arc, Italy). Contributions to Mineralogy and Petrology, 162, 275-288.

O'Leary, J.A., Rossman, G.R., and Eiler, J.M. (2007) Hydrogen analysis in minerals by continous-flow mass spectrometry. American Mineralogist, 92, 1990-1997.

O'Leary, J.A., Gaetani, G.A., and Hauri, E.H. (2010) The effect of tetrahedral Al^{3+} on the partitioning of water between clinopyroxene and silicate melt. Earth and Planetary Science Letters, doi:10.1016/j.epsl.2010.06.011.

Ottolini, L. and Hawthorne, F.C. (2001) SIMS ionization of hydrogen in silicates: a case study of kornerupine. Journal of Analytical Atomic Spectrometry, 16, 1266-1270.

Ottolini, L., Cámara, F., Hawthorne, F.C., and Stirling, J. (2002) SIMS matrix effects in the analysis of light elements in silicate minerals: comparison with SREF and EMPA data. American Mineralogist, 87, 1477-1485.

Paterson, M.S. (1982) The determination of hydroxyl by infrared absorption in quartz, silicate glasses, and similar materials. Bulletin de Minéralogie, 105, 20-29.

Peslier, A.H., Luhr, J.F., and Post, J. (2002) Low water content in pyroxenes from spinel-peridotites of the oxidized, sub-arc mantle wedge. Earth and Planetary Science Letters, 201, 69-86.

Peslier, A.H. and Luhr, J.F. (2006) Hydrogen loss from olivines in mantle xenoliths from Simcoe (USA) and Mexico: mafic alkalic magma ascent rates and water budget of the sub-continental lithosphere. Earth and Planetary Science Letters, 242, 302-319.

925 Prechtel, F. and Stalder, R. (2012) OH-defects in Al- and Cr-doped synthetic enstatites
926 and defect geobarometry on natural orthopyroxenes from the Earth's mantle.
927 European Journal of Mineralogy, 24, 471-481.
928 Rauch, M. and Keppler, H. (2002) Water solubility in orthopyroxene. Contributions to
929 Mineralogy and Petrology, 143, 525-536.
930 Rose-Koga, E.F., Shimizu, N., Devidal, J., Koga, K.T., and Le Voyer, M. (2008)
931 Investigation of F, S, and Cl standards by ion probe and electron microprobe.
932 American Geophysical Union, Fall Meeting 2008, abstract #V31B-2145.
933 Rossman, G.R. (2006) Analytical methods for measuring water in nominally anhydrous
934 minerals. In H. Keppler and J. R. Smyth, Eds., Water in Nominally Anhydrous
935 Minerals, 62, p. 1-28. Reviews in Mineralogy and Geochemistry, Mineralogical
936 Society of America, Chantilly, Virginia.
937 Schmetzer, K. and Krupp, H. (1982) Enstatite from Mairimba Hill, Kenya. Journal of
938 Gemmology, 18, 118-120.
939 Skogby, H. and Rossman, G.R. (1991) The intensity of amphibole OH bands in the
940 infrared absorption spectrum. Physics and Chemistry of Minerals, 18, 64-68.
941 Skogby, H., Bell, D.R., and Rossman, G.R. (1990) Hydroxide in pyroxene: variations in
942 the natural environment. American Mineralogist, 75, 764-774.
943 Smith, D. and Levy, S. (1976) Petrology of the Green Knobs diatreme and implications
944 for the upper mantle below the Colorado Plateau. Earth and Planetary Science
945 Letters, 29, 107-125.
946 Smith, J.V., Delaney, J.S., Hervig, R.L., and Dawson, J.B. (1981) Storage of F and Cl in
947 the upper mantle: geochemical implications. Lithos, 14, 133- 147.

948 Smyth, J.R., Frost, D.J., Nestola, F., Holl, C.M., and Bromiley, G. (2006) Olivine
949 hydration in the deep upper mantle: effects of temperature. Geophysical Research
950 Letters, 33, doi: 10.1029/2006GL026194
951 Stalder, R. (2004) Influence of Fe, Cr, and Al on hydrogen incorporation in
952 orthopyroxene. European Journal of Mineralogy, 16, 703-711.
953 Stalder, R. and Ludwig, T. (2007) OH incorporation in synthetic diopside. European
954 Journal of Mineralogy, 19, 373-380.
955 Stalder, R. and Skogby, H. (2002) Hydrogen incorporation in enstatite. European Journal
956 of Mineralogy, 14, 1139-1144.
957 Stalder, R. and Skogby, H. (2003) Hydrogen diffusion in natural and synthetic
958 orthopyroxene. Physics and Chemistry of Minerals, 30, 12-19.
959 Stalder, R., Klemme, S., Ludwig, T., and Skogby, H. (2005) Hydrogen incorporation in
960 orthopyroxene: interaction of different trivalent cations. Contributions to
961 Mineralogy and Petrology, 150, 473-485.
962 Stalder, R., Prechtel, F., and Ludwig, T. (2012) No site-specific infrared absorption
963 coefficients for OH-defects in pure enstatite. European Journal of Mineralogy, 24,
964 465-470.
965 Stalder, R., Purwin, H., and Skogby, H. (2007) Influence of Fe on hydrogen diffusivity in
966 orthopyroxene. European Journal of Mineralogy, 19, 899-903.
967 Straub, S.M. and Layne, G.D. (2003) The systematics of chlorine, fluorine, and water in
968 Izu arc front volcanic rocks: implications for volatile recycling in subduction
969 zones. Geochimica et Cosmochimica Acta 67, 4179-4203.

970 Sundvall, R. and Stalder, R. (2011) Water in upper mantle pyroxene megacrysts and
971 xenocrysts: a survey study. American Mineralogist, 96, 1215-1227.
972 Tenner, T.J., Hirschmann, M.M., Withers, A.C., and Hervig, R.L. (2009) Hydrogen
973 partitioning between nominally anhydrous upper mantle minerals and melt
974 between 3 and 5 GPa. Chemical Geology, 262, 42-56.
975 Thomas, S.-M., Koch-Müller, M., Reichart, P., Rhede, D., Thomas, R., WIrth, R., and
976 Matsyuk, S. (2009) IR calibrations for water determination in olivine, r-GeO2,
977 and SiO_2 polymorphs. Physics and Chemistry of Minerals, 36, 489-509.
978 Veblen, D.R. (1985) Direct TEM imaging of complex structures and defects in silicates.
979 Annual Reviews of Earth and Planetary Science, 13, 119-146.
980 Wade, J.A., Plank, T., Hauri, E.H., Kelley, K.A., Roggensack, K., and Zimmer, M.
981 (2008) Prediction of magmatic water contents via measurement of H_2O in
982 clinopyroxene phenocrysts. Geology, 36, 799-802.
983 Warren, J.M. and Hauri, E.H. (2010) Water concentrations in mantle peridotite minerals.
984 American Geophysical Union, Fall Meeting 2010, abstract #V23E-03.
985 Wegdén, M., Kristiansson, P., Skogby, H., Auzelyte, V., Elfman, M., Malmqvist, K.G.,
986 Nilsson, C., Pallon, J., and Shariff, A. (2005) Hydrogen depth profiling by p-p
987 scattering in nominally anhydrous minerals. Nuclear Instruments and Methods in
988 Physics Research B, 231, 524-529.
989 Williams, P. (1992) Quantitative analysis using sputtering techniques: secondary ion and
990 sputtered neutral mass spectrometry. In D. Briggs and M.P. Seah, Eds., Practical
991 Surface Analysis, p. 177-228. John Wiley & Sons Ltd, West Sussex, England.

Withers, A.C. and Hirschmann, M. (2008) Influence of temperature, composition, silica activity and oxygen fugacity on the H_2O storage capacity of olivine at 8 GPa. Contributions to Mineralogy and Petrology, 156, 595-605.

Withers, A.C., Hirschmann, M.M., and Tenner, T.J. (2011) The effect of Fe on olivine H_2O storage capacity: consequences for H_2O in the martian mantle. American Mineralogist, 96, 1039-1053.

Withers, A.C., Bureau, H., and Raepsaet, C., and Hirschmann, M.M. (2012) Calibration of infrared spectroscopy by elastic recoil detection analysis of H in synthetic olivine. Chemical Geology, 334, 92-98.

Witter, J.B. and Kuehner, S.M. (2004) A simple method for high-quality electron microprobe analysis of fluorine at trace levels in Fe-bearing minerals and glasses. American Mineralogist, 89, 57-63.

York, D. (1966) Least-squares aitting of a straight line. Canadian Journal of Physics. 44, 1079-1086.

APPENDIX 1. FTIR METHODS

Silicate overtone spectra

The dependence of polarized IR spectra in the silicate overtone region on orientation has been documented for olivine (Lemaire et al. 2004; Asimow et al. 2006) and used by several workers to verify orientations of grains for FTIR analysis. Asimow et al. (2006) derived a mathematical model for using these Si-O overtone spectra to determine H concentrations in populations of randomly oriented grains, and this method has also been used in some subsequent studies (e.g., Withers et al. 2011). In Appendix Figure 1 we show two examples of spectra in the same region for well-oriented orthopyroxene crystals, which are sometimes used in our lab as a crosscheck to confirm the orientations of crystals measured by FTIR.

Although similar spectra were already published by Prechtel and Stalder (2012), the spectra in Appendix Figure 1 demonstrate an important point: although the overall shapes of the band structures are similar for all samples studied here (and easily distinguished for the three principal orientations), differences in chemistry induce small shifts in peak locations and moderate changes to peak heights. For instance, as highlighted by the dashed line in Appendix Figure 1, the main peak in β is 10 cm^{-1} lower in GRR1650b (Mg no. 78.8, 0.73 wt% Al_2O_3) compared to KBH-1 (Mg no. 90.5, 4.67 wt% Al_2O_3); it is also significantly weaker in KBH-1, which we suggest is largely related to tetrahedral Al replacing some of the Si giving rise to these vibrations. Therefore, application of the Asimow et al. (2006) method to orthopyroxene will require either standard spectra for specific compositions close to the unknowns, or modification of the model to take composition into account. Baseline correction for these spectra is also not

as straightforward as in olivine, for which straight-line fits are easily applied with consistency between different crystals; for orthopyroxene the tail of absorbance from the fundamental Si-O vibrational region is steeper, complicating that simplistic approach. Another contribution to the uncertainty in baseline comes from the electronic transition band for Fe^{2+} in the M2 site at ~2350 cm^{-1} (Goldman and Rossman 1976), which could affect the peak heights in the silicate overtone region due to its large half-width (~1100 cm^{-1}).

Baseline correction

Aside from uncertainties in calibration, uncertainty in the baseline is by far the largest contributor to uncertainty in derived H concentrations (Bell et al. 1995; 2003). Under ideal conditions, precision of 3% or better can be achieved (Bell et al. 1995). In this study, however, we have assumed more conservative overall uncertainties, arrived at from the following considerations.

As mentioned previously, the baseline for Fe-bearing orthopyroxenes is a complex function of both Si-O vibrational bands and electronic transitions with long tails of absorption. These effects are difficult to separate for orthopyroxene, primarily because of the Fe^{2+} band at ~2350 cm^{-2} – which is absent in garnets, olivines, and clinopyroxene. This electronic transition band – which is strongest in γ, the polarization that also shows the strongest O-H absorption – has a very large full width at half height (about 1250 cm^{-1}) compared to vibrational bands, with the tail of absorption not only overlapping with the Si-O overtone region but extending as far as the frequency range of fundamental O-H vibrations. Furthermore, in β the Si-O overtones feature a strong peak at relatively high

wavenumber (linear absorbance of ~50-65/cm at ~1940 cm^{-1}; Appendix Fig. 1). The second overtones of these Si-O vibrations manifest as weak yet not trivial absorbance in the region from ~2600-3000 cm^{-1}, which interferes with the O-H bands in some samples. This phenomenon would not be significant in samples with high H concentrations, such as synthetic enstatites from high-pressure experiments, but is noticeable for samples with low H such as JLM50, which has a broad band at 3100 cm^{-1} overlapping these second overtones.

With these issues in mind, baseline correction was performed using the built-in routine in Nicolet's OMNIC software. An ideal method of baseline correction involves computer subtraction of the spectrum of a dehydrated sample from that of the sample of interest (Paterson 1982; Bell et al. 1995). In practice this is difficult for two reasons. First, strict application of this method requires dehydration of multiple samples with compositions corresponding to each wet sample, which we have not undertaken. Secondly, the dehydration process itself can induce changes in the baseline as a result of changes in oxidation state and/or site occupancy for Fe^{2+} that shift the Fe^{2+} peaks. Therefore, we performed manual correction by applying spline fits with a concave curvature, to mimic the approximate shape of the dehydrated sample spectra shown by Bell et al. (1995); these spline fits require placement of tie points below the O-H vibrational bands. We also corrected by eye for the absorption caused by the second Si-O overtones in β explained above. Finally, we subtracted the estimated component in β corresponding to hydrous phase inclusions (amphibole and/or talc and/or serpentine). This last correction is only unambiguous for the one sample (GRR1650b) that showed sharp bands at 3675 cm^{-1} and 3662 cm^{-1}, well separated from the intrinsic O-H bands in

this orientation. Fortunately the correction for hydrous phases is small overall for all samples, as a result of the low absorbance in this direction compared to γ and α.

The corrections outlined above entail unavoidable subjectivity. Rather than assign a blanket uncertainty to the absorbance, as in previous studies (e.g., Mosenfelder et al. 2011), we also performed a subjective evaluation of uncertainties for each individual spectrum, taking into account the various factors described above. An upper bound on this uncertainty for a given spectrum can be calculated from the difference between the curved fit we chose and a simple linear fit between the bounding points of the integration. This discrepancy can be as high as 30% and is clearly unrealistically high in most cases. Our final estimates of uncertainties in absorbance range from 7 to 25% for individual spectra, as reflected in Table 1; when propagated in order to calculate total absorbance (in three directions) by summing in quadrature, the final uncertainties range from 6 to 12%. Further propagation with the uncertainty in the molar absorption coefficient, as described in the analytical methods section, results in final uncertainties in H concentrations of 10 to 14%.

Tables

Table 1. FTIR data for orthopyroxene

Table 2. Calibration data for fluorine

Table 3. EPMA data for orthopyroxene

Table 4. SIMS data for orthopyroxene and olivine

Appendices (Online Support Material)

1099 **Appendix 1.** SIMS analyses

1100 **Appendix 2.** FTIR spectra

1101

1102 **Figure Captions**

1103 **Figure 1.** Polarized IR spectra of orthopyroxenes in the

1104 α, β, □□□ γ □□□□□□□□□□□□□̃Sample numbers are labeled directly above each

1105 spectrum. All spectra normalized to 1 cm, shown without baseline correction, and offset

1106 for clarity.

1107

1108 **Figure 2.** IR spectra of selected orthopyroxenes and hydrous minerals. Spectra

1109 normalized to different thicknesses and offset for ease of comparison. Normalized

1110 thicknesses and polarizations shown in brackets next to sample label. The thickness of the

1111 spectrum of serpentine (Miller et al. 1987) is arbitrary as it was embedded in a KBr

1112 pellet.

1113

1114 **Figure 3. a.** Comparison of H concentrations in orthopyroxene determined using the

1115 calibrations of Bell et al. (1995) and Libowitzky and Rossman (1997)(L&R), as a

1116 function of the ratio of low to high wavenumber absorbance (see Table 1). **b.** Overall

1117 comparison of the two calibrations. Ordinary least squares (OLS) regression shown for

1118 our data only; data from Sundvall and Stalder (2011) also shown for comparison.

1119

1120 **Figure 4.** SIMS calibration for F. All data shown are blank corrected. GRR1017, at the

1121 origin, was included in all regressions. Solid black lines are OLS regressions, with

equations shown; grey lines are York regressions, with 95% confidence intervals shown as dashed lines. **a.** Data for MPI-DING (excluding ATHO-G) and NIST glasses assuming F values from Jochum et al. (2006). Error bars on F represent ±10% uncertainty; error bars in normalized isotopic ratios are 2σ. **b.** Data for four basalts (solid circles), assuming values for F from Guggino and Hervig (2011). Also shown are data for NIST SRM 610 and NIST SRM 612 (open circles), assuming values from Guggino and Hervig (2010). The NIST glasses were not included in the regressions.

Figure 5. Correlation between $^{16}O^{1}H/^{30}Si$ and $^{19}F/^{30}Si$ for selected samples. 2σ error bars are within the symbol size for all data points. Ratios in this graph are raw, not blank corrected. Sample numbers are labeled next to data clusters. Regression line ($r^2 = 0.999$) is shown for sample JLM14 only; for that sample we also include an analysis from an earlier SIMS session (March, 2010) that yielded very high $^{16}O^{1}H/^{30}Si$ and $^{19}F/^{30}Si$. For the sake of the regressions shown in Figure 5, data averaged for samples JLM14 and JLM46 were restricted to analyses with $^{19}F/^{30}Si \leq 0.0032$ or 0.0048, respectively.

Figure 6. SIMS calibration for H in orthopyroxene. All data shown are blank corrected; error bars are 2σ. Solid black lines are OLS regressions, with equations shown. Grey lines are York regressions, with 95% confidence intervals shown as dashed lines. **a.** Calibration assuming Bell et al. (1995) IR calibration. **b.** Calibration assuming Libowitzky and Rossman (1997) IR calibration. The lower confidence interval is nearly coincident with the OLS regression. Arrows point to two samples showing the most difference in calculated H concentration between the two different IR calibrations.

1145

1146 **Figure 7.** Alumina concentration versus F (model 2) in orthopyroxene, demonstrating
1147 overall lack of correlation. Data from this study (closed circles) shown together with
1148 three analyses (open circles) by Beyer et al. (2012) of natural orthopyroxenes. The latter
1149 do show a good correlation between Al_2O_3 and F when considered alone. Also shown are
1150 experimental data from Dalou et al. (2012)(open diamonds) and Beyer et al. (2012)(open
1151 squares).

1152

1153 **Figure 8.** SIMS calibration for H in olivine (solid squares) compared to calibration for
1154 orthopyroxene from Figure 6a (open circles). Values for ppm H_2O are based on NRA or
1155 FTIR data (details in Mosenfelder et al. 2011). Error bars (2σ□□) shown for olivine but
1156 omitted for orthopyroxene for the sake of clarity. Solid black line is the OLS regression,
1157 with equation shown. Grey line is the York regression, with 95% confidence intervals
1158 shown as dashed lines.

1159

1160 **Appendix Figure 1.** Representative IR spectra of orthopyroxenes in the silicate overtone
1161 region. All spectra normalized to 1 cm, presented without baseline correction, and offset
1162 for clarity. Upper (black line) and lower (grey line) spectra for each direction are from
1163 KBH-1 or GRR1650b, respectively. The slabs cut to measure these spectra were thinned
1164 to less than 200 μm in order to reduce relevant peak heights to an absorbance less than
1165 two. Dashed line highlights a shift in the strong peak at ~1940-1950 cm^{-1} in β (the
1166 same □□□□□is □□□□□□□□□for this peak □□ α).

1167

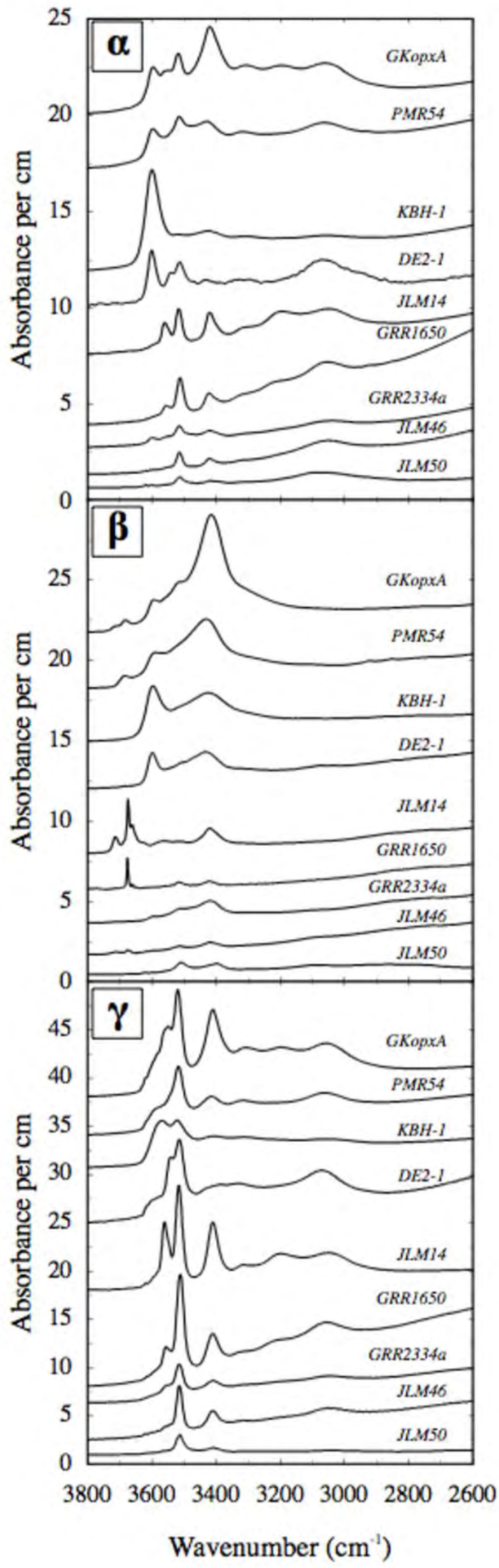

Mosenfelder et al., Fig. 1

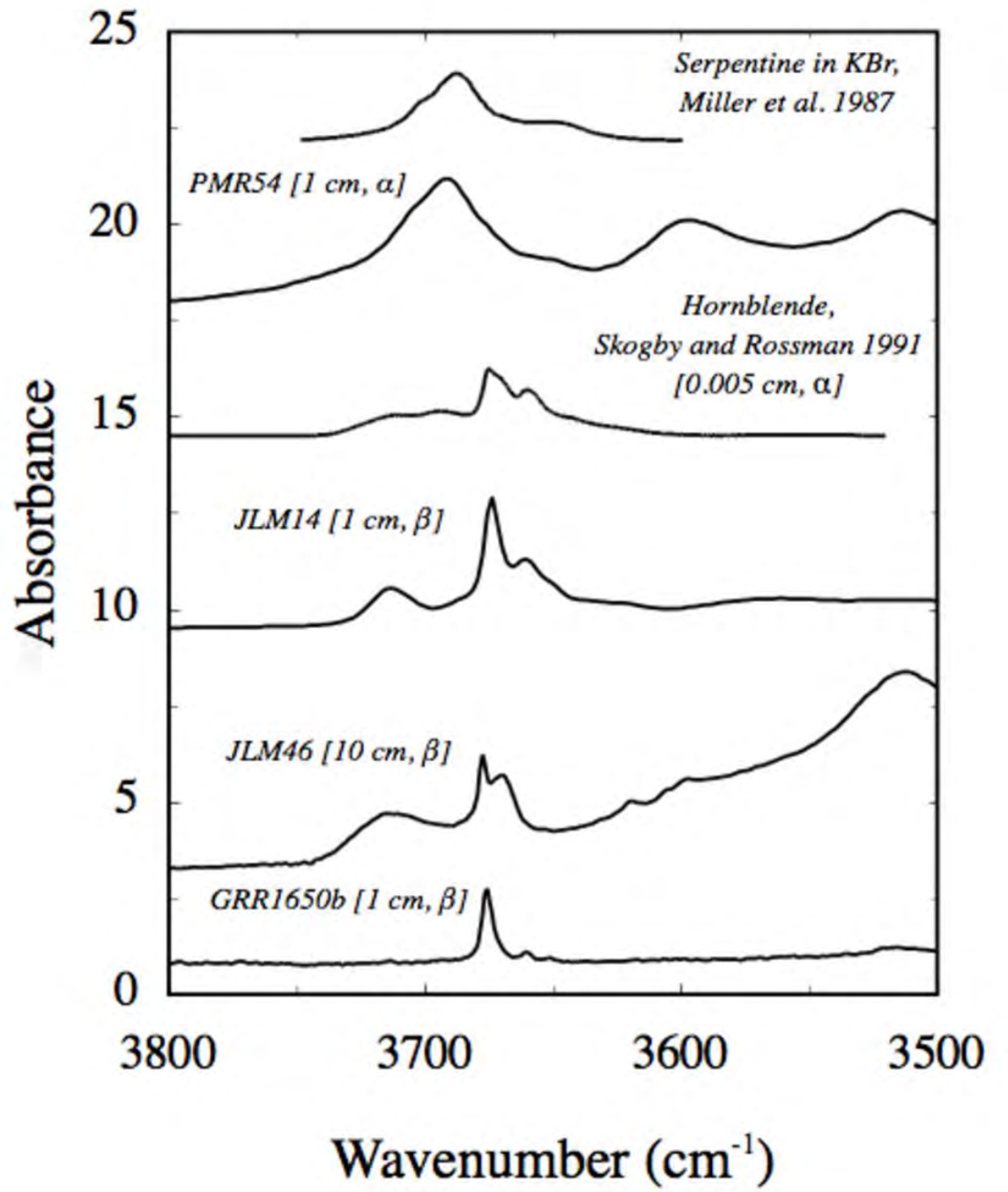

Mosenfelder et al., Fig. 2

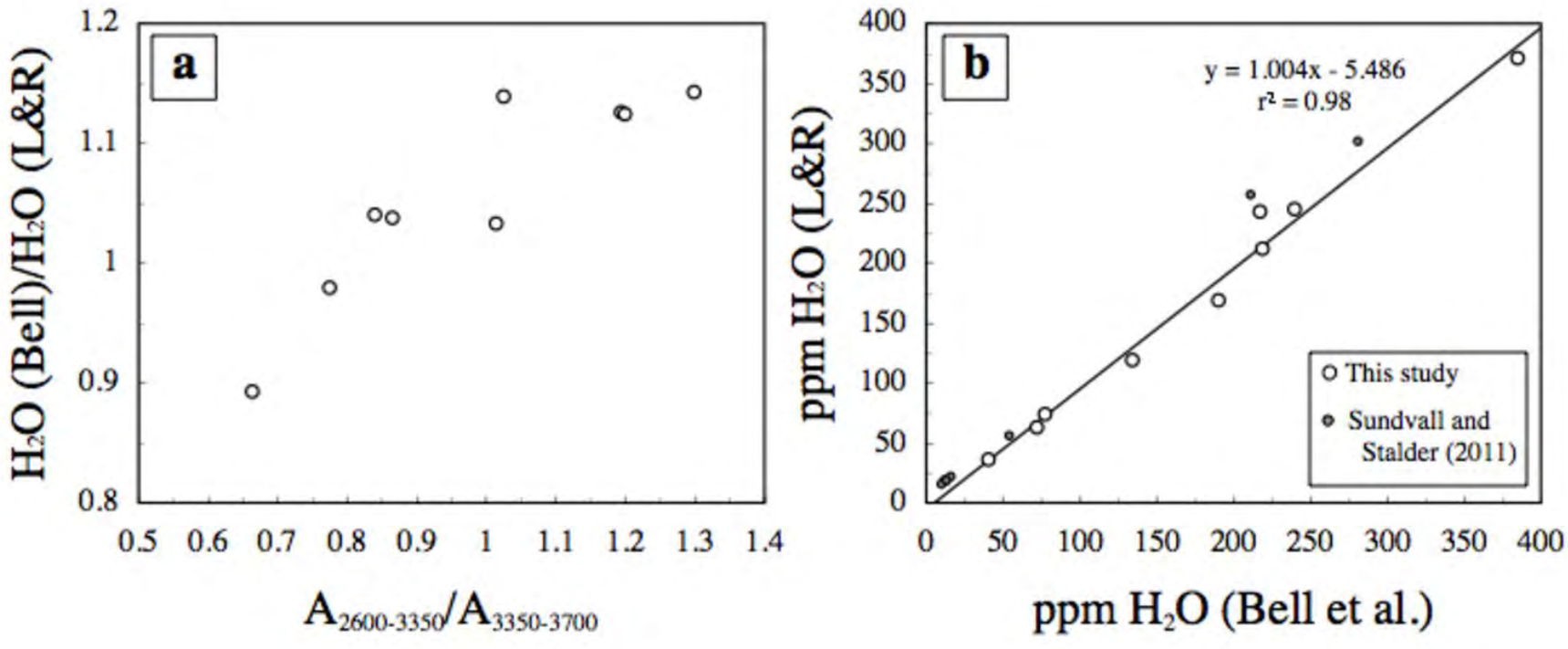

Mosenfelder et al., Fig. 3

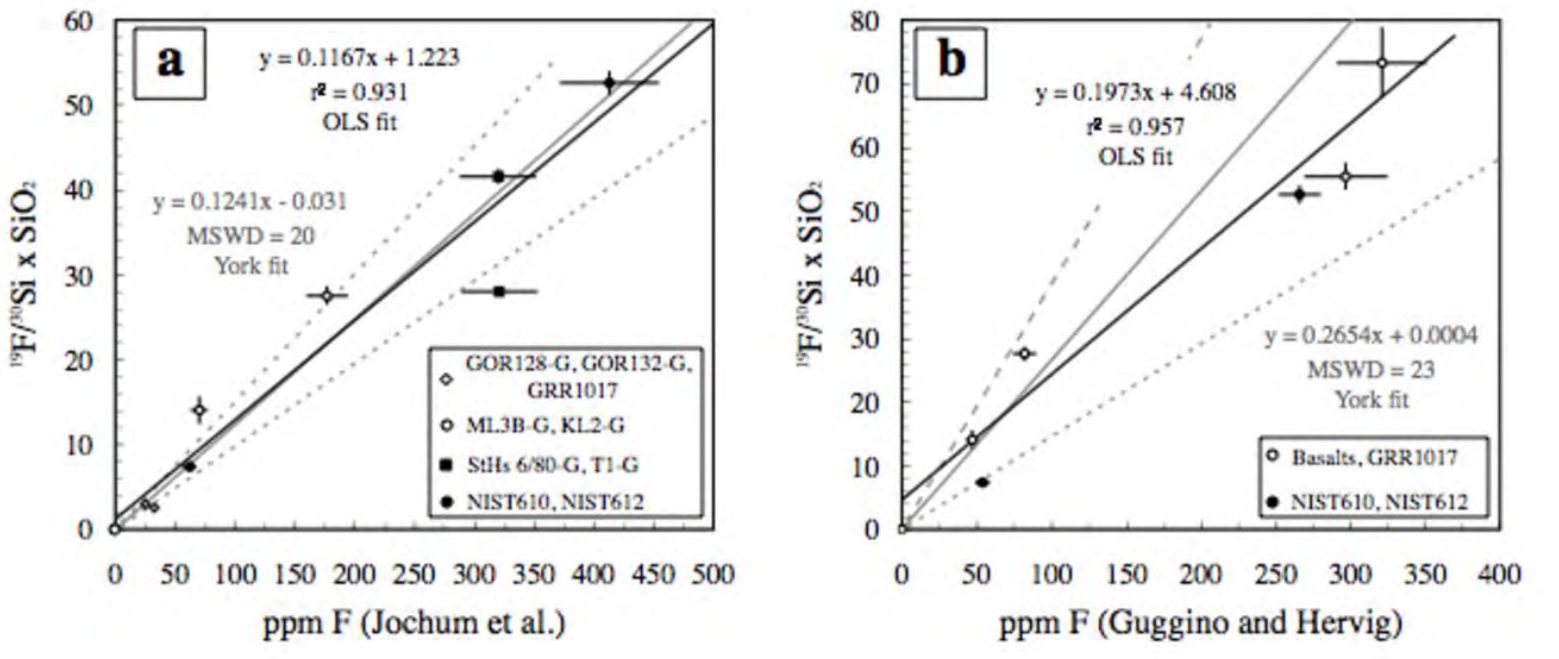

Mosenfelder et al., Fig. 4

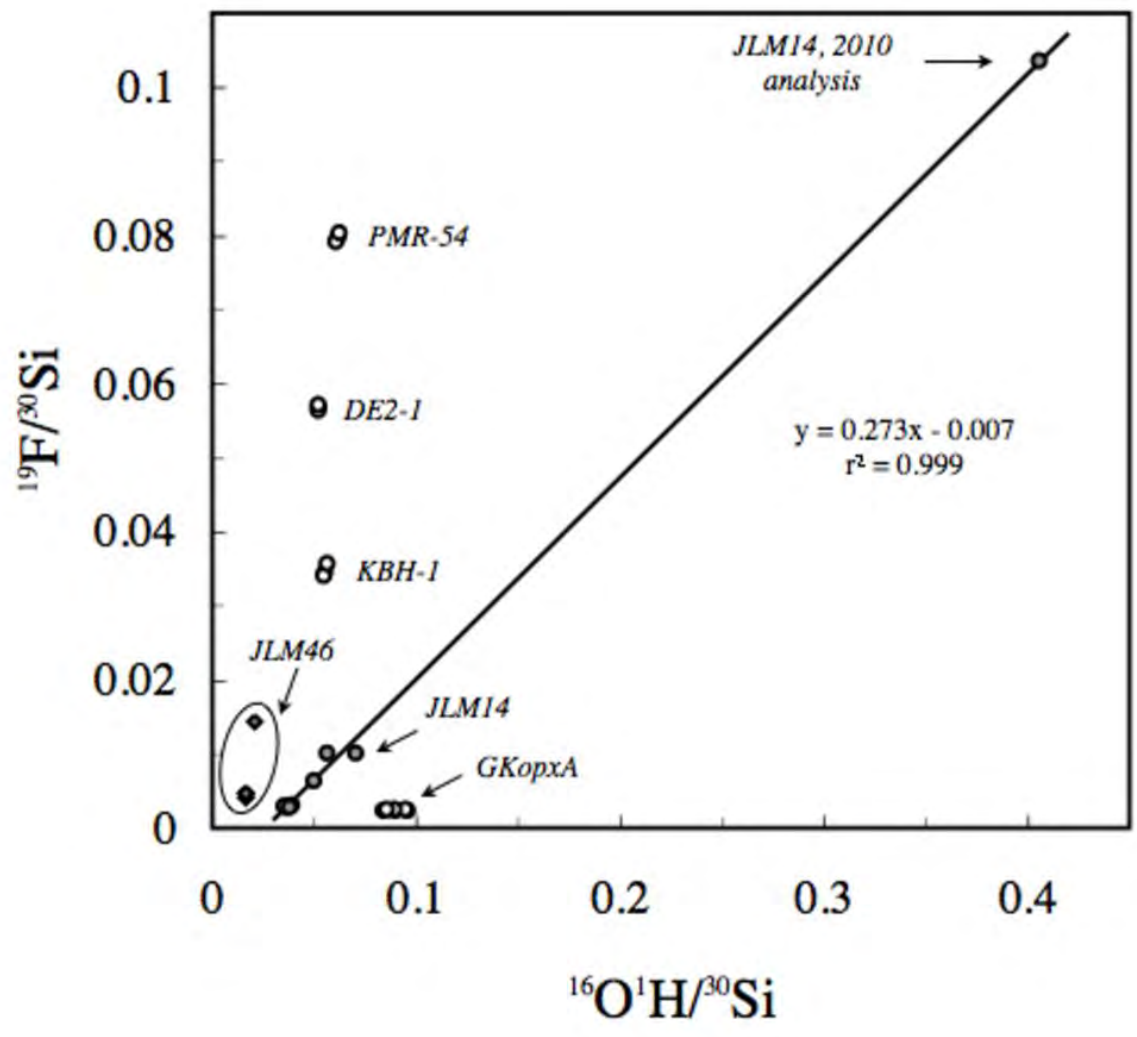

Mosenfelder et al., Fig. 5

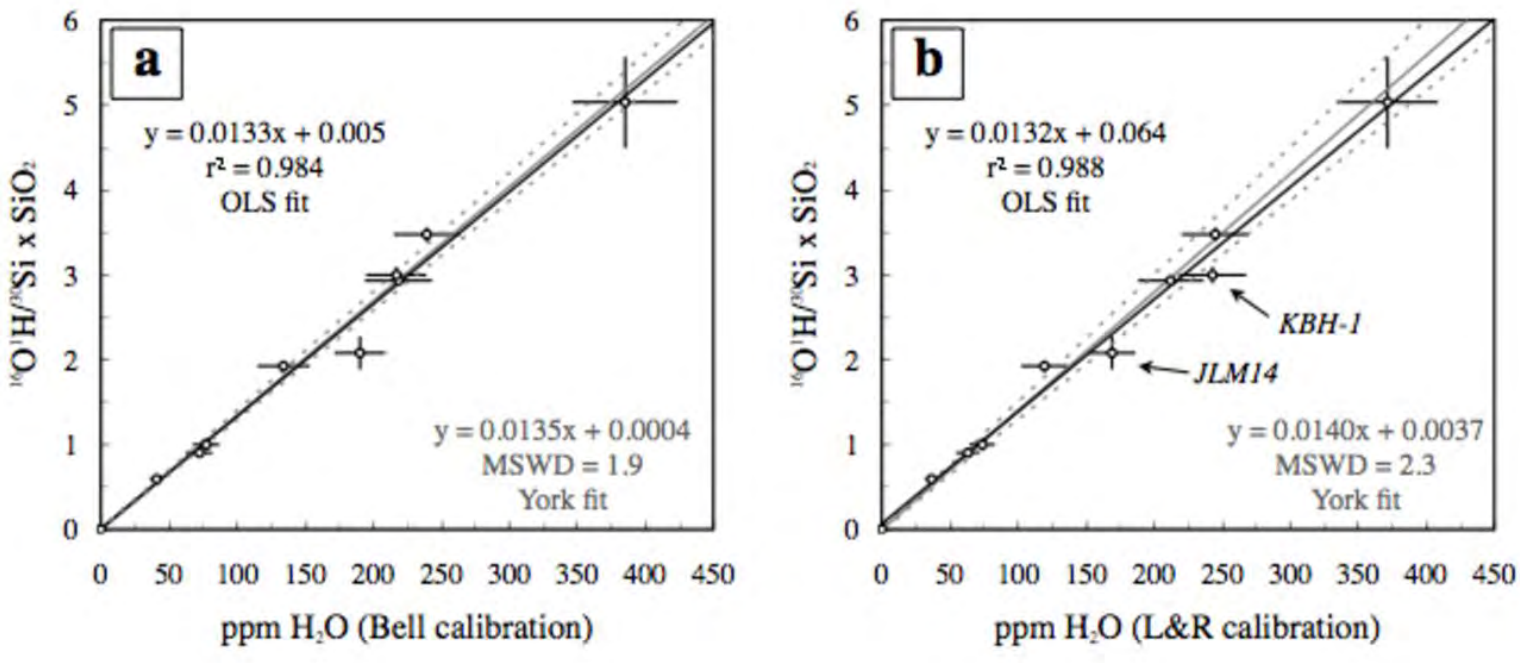

Mosenfelder et al., Fig. 6

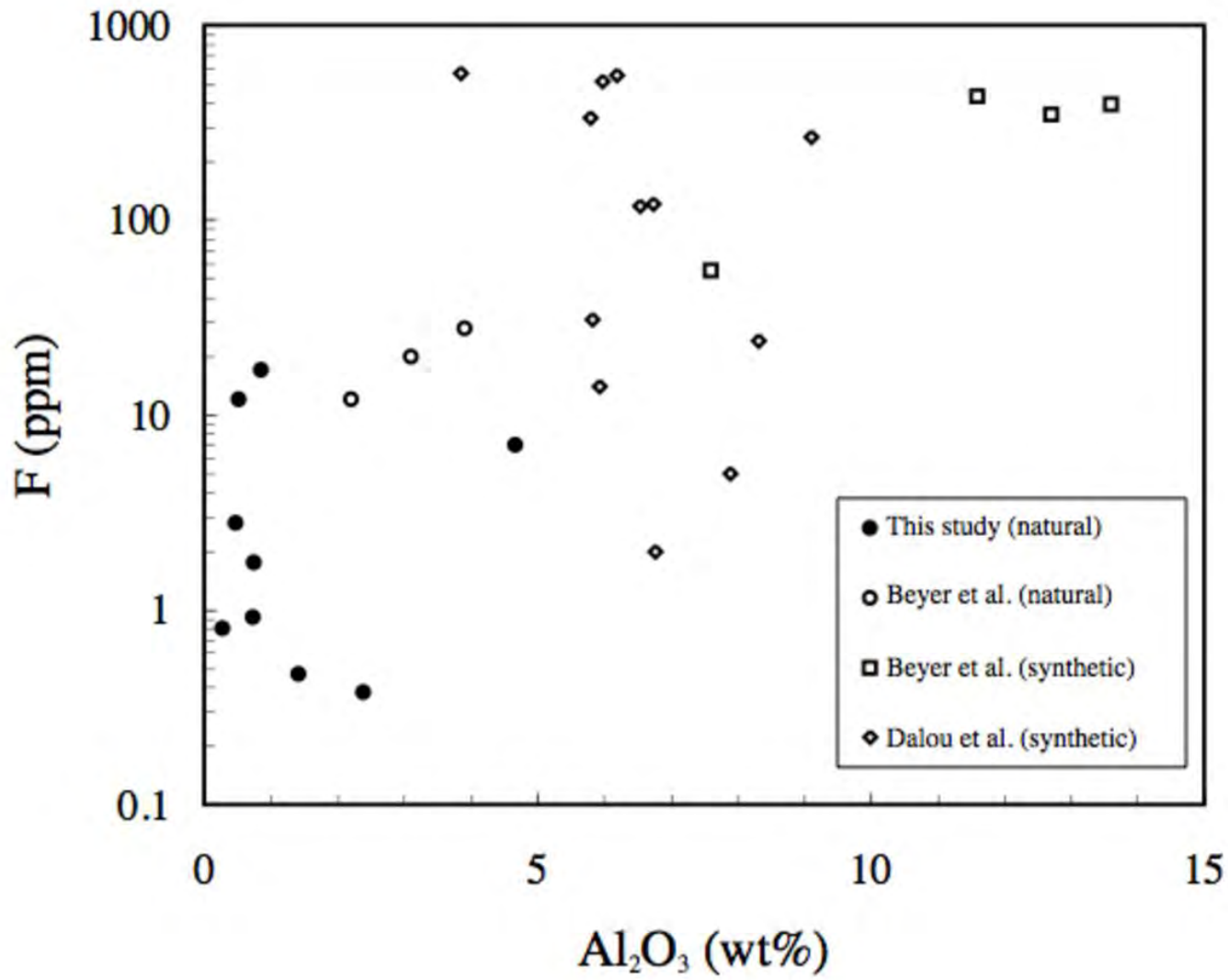

Mosenfelder et al., Fig. 7

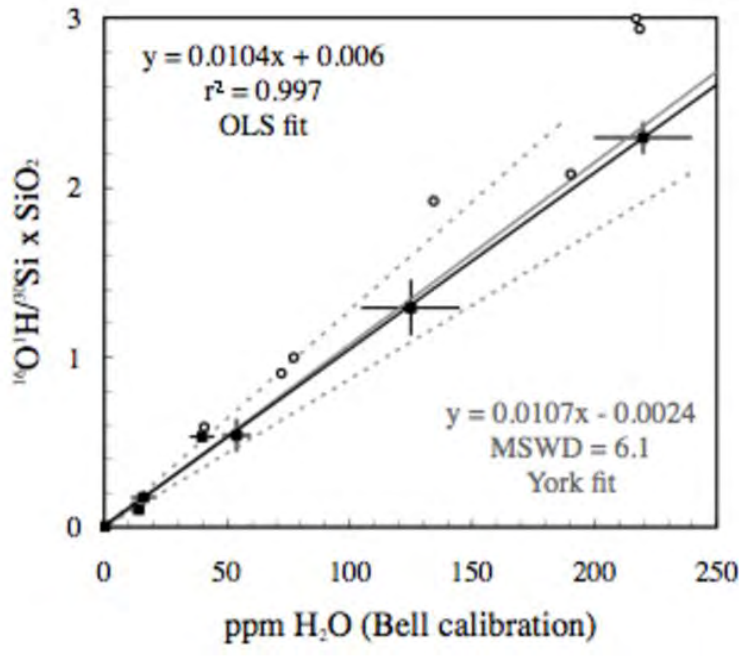

Mosenfelder et al., Fig. 8

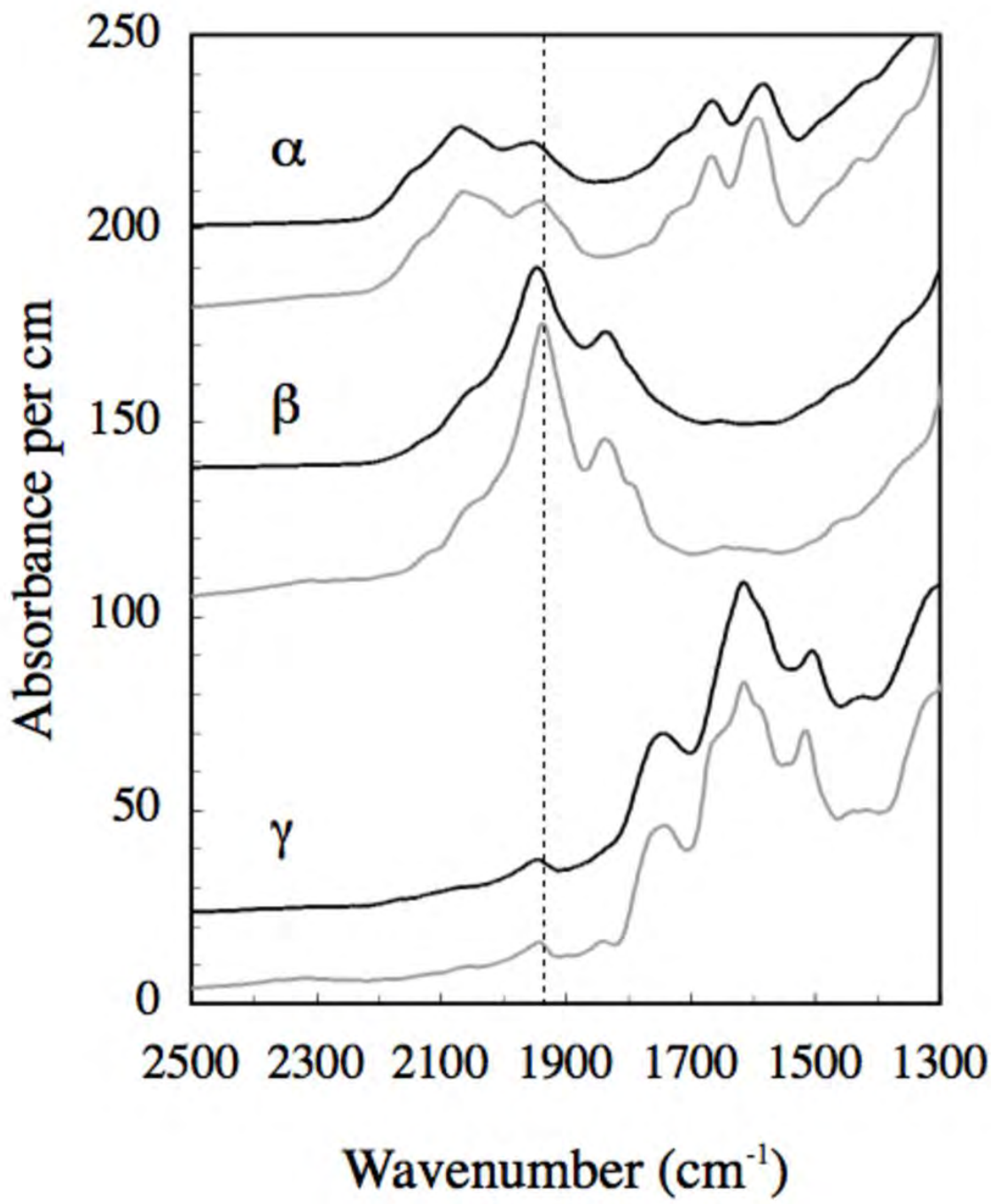

Mosenfelder et al., Fig. A1

Table 1. FTIR data for orthopyroxene

Sample no.	Locality	Density	IR integrated absorbance/cm						H_2O, Bell	H_2O, L&R	References
		Mg/m^3 (2s)	a	b	g	A (2600-3350 cm^{-1})	A (3350-3700 cm^{-1})	A (total)	(ppm by weight)	(ppm by weight)	
ZM1opx-HT	Kilbourne Hole, New Mexico, U.S.A. (dehydrated)	-	0	0	0	0	0	0	0	0	This study
GRR247	Synthetic	-	0	0	0	0	0	0*	0	0	Ito (1975)
JLM50	unknown **	3.210(1)	226(27)	113(23)	247(42)	297	289	586(55)	41(5)	36(4)	This study
JLM46	Tanzania	3.271(2)	245(32)	82(12)	730(109)	597	460	1057(115)	72(10)	63(8)	This study; Beran and Zemann (1986)
GRR2334a	Mogok area, Myanmar	3.275(1)	245(49)	231(35)	657(99)	517	616	1134(115)	77(10)	74(10)	This study
GRR1650b	India	3.301(1)	404(48)	34(3)	1547(232)	1080	905	1985(237)	134(19)	119(17)	Skogby et al. (1990)
JLM14	Tanzania	3.279(1)	684(89)	136(34)	1974(138)	1524	1271	2794(168)	190(19)	169(17)	This study; Beran and Zemann (1986)
KBH-1	Kilbourne Hole, New Mexico, U.S.A.	3.318(17)	802	990	1434	1287	1939	3226***	217(22)****	243(25)	Bell et al. (1995)
DE2-1	Deutsche Erde 2 kimberlite, Gibeon kimberlite province, Namibia	3.318*	845(110)	468(56)	1935(232)	1635	1612	3248(263)	219(25)	212(24)	This study; Mitchell (1987)
PMR-54	Premier Mine, S. Africa	3.318*	929(93)	987(118)	1642(164)	1553	2005	3558(223)	240(24)	245(25)	Skogby et al. (1990)

GKopxA	Green Knobs, Arizona, U.S.A.	3.318*	1403(98)	1357(163)	2963(296)	2654	3069	5723(352)	385(39)	371(37)	This study; Smith and Levy (1976)

Notes: Bands corresponding to hydrous phase inclusions were subtracted from absorbance. "Bell" and "L&R" refer to calibrations by Bell et al. (1995) and Libowitzky and Rossman (1997), respectively

*Some spectra showed a weak broad band at 3400 cm^{-1}; see text

**Country of origin might be either Kenya or Tanzania, based on comparison to color, chemical, and density data provided by Jackson (1982) and Beran and Zemann (1986), respectively

***Integration well within uncertainty of originally published value (3221±115)

****Value and uncertainty (2s) are from hydrogen manometry (Bell et al. 1995); uncertainty on other samples estimated as discussed in text

Table 2. Calibration data for fluorine

Sample No.	SiO_2* wt%	No. Analyses	$^{19}F/^{30}Si$**	F (ppm)	Reference for fluorine content
	Forsterite (blank standard)				
GRR1017	42.69	4	0.0111(5)	0	This study
	USGS glasses				
BCR-2G	54.8	4	1.34(10)	321(30)	Guggino et al. (2011)
BHVO-2G	49.3	3	1.13(4)	297(28)	Guggino et al. (2011)
	MPI-DING glasses				
GOR128-G	46.1	3	0.065(2)	25(3)	Jochum et al. (2006)
GOR132-G	45.5	3	0.057(1)	32(3)	Jochum et al. (2006)
KL2-G	50.3	7	0.55(2)	177(18)	Jochum et al. (2006)
				82(8)	Guggino et al. (2011)
ML3B-G	51.4	7	0.27(3)	70(7)	Jochum et al. (2006)
				47(4)	Guggino et al. (2011)
T1-G	58.6	3	0.478(7)	321(32)	Jochum et al. (2006)
				220(7)	Guggino et al. (2010)
StHs 6/80-G	63.7	3	0.65(1)	320(32)	Jochum et al. (2006)
				278(2)	Guggino et al. (2010)
ATHO-G	75.6	3	2.32(7)	0.70(7)	Jochum et al. (2006)
	NIST glasses				
NIST SRM 610	72.276	3	0.73(2)	500	Nominal NIST value
				295(32)	Hoskin (1999)
				611(202)	Straub and Layne (2003)
				413(41)	Jochum et al. (2006)
				266(14)	Guggino et al. (2010)
NIST SRM 612	71.79	3	0.102(2)	50	Nominal NIST value
				122(34)	Straub and Layne (2003)
				62(6)	Jochum et al. (2006)
				54(5)	Guggino et al. (2010)

Uncertainties (in parentheses) are $2s_{SD}$, except for values from Jochum et al. (2006), which represent a combined reproducibility/accuracy of 10%

*Preferred values from Jochum et al. (2005), Jochum et al. (2006), and Pearce et al. (1997) for USGS, MPI-DING, and NIST glasses respectively

**$^{19}F/^{30}Si$ ratios are blank corrected, except for GRR1017 (average of raw values)

Table 3: EPMA data for orthopyroxene

Sample no.	ZM1opxHT	GRR247	JLM50	JLM46	GRR2334a	GRR1650b	JLM14	DE2-1	KBH-1	PMR-54	GKOPXa
No. analyses	4	5	4	4	3	4	7	4	3	4	4
SiO_2	55.79(21)	55.58(33)	59.53(15)	58.06(12)	57.70(4)	55.49(16)	57.08(27)	57.07(24)	54.51(23)	56.99(5)	56.32(19)
TiO_2	0.06(1)	n.d.	n.d.	0.04(1)	0.04(1)	0.06(2)	n.d.	0.17(1)	0.11(1)	0.26(2)	n.d.
Al_2O_3	2.81(2)	n.d.	0.47(1)	0.28(1)	0.75(1)	0.73(2)	1.42(3)	0.51(1)	4.67(2)	0.85(1)	2.39(5)
FeO	6.11(5)	n.d.	0.79(2)	5.97(4)	5.95(4)	13.86(10)	6.07(5)	8.34(6)	6.03(4)	6.85(2)	5.24(6)
MgO	33.06(11)	28.05(39)	39.00(8)	35.17(7)	34.94(3)	28.94(5)	34.84(22)	32.77(5)	32.33(12)	33.26(4)	34.47(1)
CaO	0.87(1)	n.d.	0.19(1)	0.16(1)	0.56(2)	0.32(1)	0.30(4)	0.62(2)	0.88(1)	0.88(1)	0.14(2)
Na_2O	0.05(1)	n.d.	n.d.	0.04(1)	n.d.	n.d.	n.d.	0.08(1)	0.12(2)	0.16(1)	n.d.
Cr_2O_3	0.60(2)	n.d.	n.d.	n.d.	0.16(1)	0.02(1)	n.d.	0.05(1)	0.51(1)	0.10(1)	0.51(1)
MnO	0.13(1)	n.d.	0.08(1)	0.23(1)	0.101(1)	0.28(1)	0.17(1)	0.15(1)	0.13(1)	0.12(1)	0.14(1)
V_2O_3	0.02(1)	0.20(1)	n.d.	n.d.	n.d.	n.d.	n.d.	n.d.	n.d.	n.d.	n.d.
NiO	0.11(3)	0.13(3)	n.d.	n.d.	0.12(1)	0.09(2)	0.09(2)	n.d.	0.12(1)	0.09(3)	0.08(2)
CoO	n.a.	16.01(44)	n.a.	n.a.	n.a.	n.a.	n.a.	n.a.	n.a.	n.a.	n.a.
Total	99.62	99.96	100.05	99.96	100.32	99.77	99.97	99.75	99.41	99.56	99.29
Mg# *	90.6	100.0	98.9	91.3	91.3	78.8	91.1	87.5	90.5	89.6	92.1

Notes: n.d. = not detected; n.a. = not analyzed; P and K were also analyzed and below detection limit in all samples

* Mg# = 100 x molar Mg/(Mg+Fe)

Table 4: SIMS data for orthopyroxene and olivine

Sample No.	No. Analyses	$^{16}O^{1}H/^{30}Si$	$^{19}F/^{30}Si$	Fluorine (ppm) * Model 1	Model 2
	Orthopyroxenes				
ZM1opx-HT	4	*0.0006(1)*	0.0446(191)	20(9)	9(4)
GRR247	3	0.0011(1)	*0.00072(3)*	0	0
JLM50	3	0.0099(5)	0.0125(4)	6.2(4)	2.80(9)
JLM46	4	0.0167(45)	0.0063(99)	**	**
	3***	0.0156(1)	0.0038(7)	2.0(6)	0.8(2)
GRR2334a	3	0.0173(13)	0.0081(2)	4.0(3)	1.76(4)
GRR1650b	4	0.0346(12)	0.0044(2)	2.2(3)	0.92(4)
JLM14	7	0.0457(262)	0.0048(68)	**	**
	4****	0.0364(34)	0.0022(3)	1.3(4)	0.47(6)
KBH-1	3	0.0550(17)	0.0340(17)	15(1)	7.0(3)
DE2-1	3	0.0514(4)	0.0561(8)	26.0(6)	12.1(2)
PMR-54	3	0.0609(15)	0.0791(13)	36.6(8)	17.0(3)
GKopxA	6	0.0893(96)	0.0018(1)	1.1(3)	0.38(2)
	Olivines				
GRR1017	4	*0.00044(7)*	*0.00088(11)*	0	0
GRR997	1	0.00077(4)	0.0057(2)	2.1(3)	0.88(3)
GRR999a	3	0.00247(5)	0.0120(5)	4.2(4)	1.84(8)
GRR1695-2	4	0.0044(9)	0.0020(26)	**	**
GRR1629-2	3	0.0130(5)	0.0031(2)	1.3(3)	0.47(3)
GRR1784e	3	0.0132(24)	0.0049(3)	1.9(3)	0.75(4)
ROM177	5	0.0332(43)	0.2533(93)	80(3)	37(1)
GRR1012-2	5	0.0660(236)	0.3042(89)	100(3)	47(1)
	2*****	0.0561(23)	0.3043(111)	100(4)	47(2)

All values blank corrected except for values in italics for ZM1opx-HT, GRR247, and GRR1017
Uncertainties (in parentheses) are $2s_{SD}$, except for GRR997 ($2s_{mean}$)
Uncertainties in F content do not take into account uncertainties in calibration

* models 1 and 2 described in the text

**$2s_{SD}$ is larger than average value

***excluding one analysis with $^{19}F/^{30}Si = 0.0137$

****excluding three analyses with $^{19}F/^{30}Si > 0.0025$

*****excluding three analyses with $s_{mean}/s_{Poisson} > 5$, see Mosenfelder et al. (2011)